Cytomegalovirus restricts ICOSL expression on antigen presenting cells disabling T cell co-stimulation and contributing to immune evasion

Angulo, Guillem; Železnjak, Jelena; Martínez-Vicente, Pablo; Puñet-Ortiz, Joan; Hengel, Hartmut; Messerle, Martin; Oxenius, Annette; Jonjić, Stipan; Krmpotić, Astrid; Engel, Pablo; ...

Cytomegalovirus restricts ICOSL expression on antigen presenting cells disabling T cell co-stimulation and contributing to immune evasion

Guillem Angulo[1†], Jelena Zeleznjak[2,3†], Pablo Martínez-Vicente[1,4], Joan Puñet-Ortiz[1,4], Hartmut Hengel[5,6], Martin Messerle[7], Annette Oxenius[8], Stipan Jonjic[2,3], Astrid Krmpotić [3], Pablo Engel[1,4], and Ana Angulo[1,4*]

[1]Immunology Unit, Department of Biomedical Sciences, Faculty of Medicine and Health Sciences, University of Barcelona, Barcelona 08036, Spain

[2]Center for Proteomics, Faculty of Medicine, University of Rijeka, Rijeka 51000, Croatia

[3]Department of Histology and Embryology, Faculty of Medicine, University of Rijeka, Rijeka 51000, Croatia

[4]Institut d'Investigacions Biomèdiques August Pi i Sunyer, Barcelona 08036, Spain

[5] Institute of Virology, University Medical Center, Albert-Ludwigs-University Freiburg, 79104 Freiburg, Germany

[6]Faculty of Medicine, Albert-Ludwigs-University Freiburg, 79104 Freiburg, Germany

[7]Institute of Virology, Hannover Medical School, Hannover 30625, Germany

[8]Institute of Microbiology, Department of Biology, ETH Zürich, Zürich, Switzerland

*Corresponding author: aangulo@ub.edu

†These authors contributed equally to this work

Short Title: MCMV decreases T-cell activation by downregulating ICOSL expression

Abstract

Viral infections are controlled, and very often cleared, by activated T lymphocytes. The inducible co-stimulator (ICOS) mediates its functions by binding to its ligand ICOSL, enhancing T-cell activation and optimal germinal center (GC) formation. Here, we show that ICOSL is heavily downmodulated during infection of antigen presenting cells by different herpesviruses. We found that, in murine cytomegalovirus (MCMV), the immunoevasin m138/fcr-1 physically interacts with ICOSL, impeding its maturation and promoting its lysosomal degradation. This viral protein counteracts T-cell responses, in an ICOS-dependent manner, and limits virus control during the acute MCMV infection. Additionally, we report that blockade of ICOSL in MCMV-infected mice critically regulates the production of MCMV-specific antibodies due to a reduction of T follicular helper and GC B cells. Altogether, these findings reveal a novel mechanism evolved by MCMV to counteract adaptive immune surveillance, and demonstrates a role of the ICOS:ICOSL axis in the host defense against herpesviruses.

Introduction

A robust host response against viral infections requires the activation of the adaptive arm of the immune system mediated by T lymphocytes. For effective T-cell activation, in addition to the antigen-specific signal delivered by the interaction of major histocompatibility (MHC)-peptide complexes and T-cell receptors (TCR), concerted co-stimulatory signals are essential. These signals come from a number of co-stimulatory molecules upon interaction with their cognate ligands, expressed on antigen-presenting cells (APCs) (Sharpe, 2009; Chen and Flies, 2013). The B7-CD28 family of ligands and receptors comprises molecules of the Ig superfamily that function as co-signaling molecules modulating T-cell responses (Sharpe and Freeman, 2002). The best characterized co-stimulatory pathway between members of this family is exemplified by the T-cell surface receptor CD28, which binds to the activated APC surface molecules B7-1 (CD80) and B7-2 (CD86). Another co-stimulatory pathway of this family is the receptor ICOS (inducible co-stimulator, CD278), primarily expressed on activated T cells and at very high levels on T follicular helper cells (Tfh), which mediates its functions by binding to its ligand ICOSL (B7-H2, CD275) (Hutloff et al., 1999; Yoshinaga et al., 1999). ICOSL is constitutively expressed on APCs, such as dendritic cells (DCs), macrophages and B cells, and it is strongly up-regulated by inflammatory stimuli (Aicher et al., 2000; Swallow et al., 1999; Yoshinaga et al., 2000). ICOSL presents a different expression profile as compared to CD80 and CD86, and it is induced on non-lymphoid cells, such as endothelial cells or epithelial cells (Khayyamian et al., 2002; Qian et al., 2006). The ICOS:ICOSL receptor pathway leads to enhanced T-cell activation, proliferation, and Th2 responses (Riley et al., 2002; Tesciuba et al., 2001). In contrast to CD28, which is essential for the activation of

naïve T cells, ICOS is more relevant for the regulation of activated and effector T cells (Coyle et al., 2000). In addition, ICOS co-stimulation plays an essential role in T-dependent antibody responses and germinal center (GC) formation, by inducing IL-21 production and Bcl6 expression, consequently controlling isotype switching, somatic hypermutation, and the generation of memory B cells and plasma cells (Choi et al., 2011; Hutloff, 2015; Liu et al., 2015). ICOS has also been shown to be required for optimal $CD8^+$ T-cell proliferation and cytokine production during recall responses (Takahashi et al., 2009; Wallin et al., 2001) and NK cell activation (Ogasawara et al., 2002). Importantly, although the ICOSL:ICOS axis is a crucial tuner of cell-mediated immune responses, little is known about its role in viral host defence.

Throughout the process of pathogen-host coevolution, viruses have devised multiple strategies to counteract host immunity. In particular, in order to ensure their prolonged survival in their hosts, persistent viruses need to undermine adaptive immune responses at different levels. A common theme of these viruses is to interfere with the presentation of antigenic peptides by MHC molecules to T cells. To this end, several large DNA viruses, particularly herpesviruses, encode multiple proteins, which usually are not essential for replication *in vitro*, with the capacity to interfere with the MHC molecules or additional cellular components involved in antigen presentation pathway (Schuren et al., 2016). Given the importance of APCs in triggering and maintenance of adaptive antiviral immune responses, herpesviruses have evolved molecular determinants and mechanisms to impair their functions (Brinkmann et al., 2015; Gewurz et al., 2007). Among them, different members of the herpesvirus family have been reported to disrupt the interaction established by co-signaling molecules in infected APCs and their counter receptors, in particular by downregulating CD80 and CD86. This is the case for

example of the human and murine cytomegaloviruses (HCMV and MCMV, respectively), which cause the downregulation of these two molecules during their respective infectious courses (Hertel et al., 2003; Loewendorf et al., 2004; Mintern et al., 2006; Moutaftsi et al., 2002). However, whether viruses have evolved immune evasion strategies to counteract the ICOSL:ICOS pathway remains largely unexplored.

Here we report that ICOSL-mediated co-stimulation contributes to the development of effective anti-MCMV immune responses. In addition, we demonstrate that ICOSL constitutes a major target of CMVs and other herpesviruses, which potently downregulate its expression on the surface of APCs. We show that MCMV uses its immunoevasin m138/fcr-1 to manipulate this co-signaling molecule, impeding a correct T-cell activation during acute MCMV infection. These results reveal a new mechanism of viral immune evasion.

Results

MCMV infection rapidly induces a potent ICOSL downregulation in APCs

ICOSL is constitutively expressed at high levels on APCs, including DCs and macrophages, which are cell types that are susceptible to MCMV infection. In order to evaluate whether MCMV has the capacity to alter cell-surface expression of ICOSL, we initially mock-infected or infected murine peritoneal macrophages, at a multiplicity of infection (moi) of 10, with a GFP expressing MCMV (MCMV-GFP). Under these conditions, around 50% of the cells in the culture were infected. Three days later, cultures were analyzed by flow cytometry to measure the expression of cell surface ICOSL. At this time point, as expected, the density of MHC I at the cell surface was strongly reduced (Figure 1A). Notably, a pronounced downmodulation of ICOSL was also observed in GFP+ infected cells as compared with uninfected GFP- cells from the same cultures, or with mock-infected samples (Figure 1A). Indeed, ICOSL levels decreased to almost undetectable levels, whereas the expression of the adhesion molecule CD62L, used as a negative control, remained unaffected. We next assessed if these findings could be extended to primary bone-marrow-derived macrophages (BMM) and dendritic cells (BMDC). Importantly, while robust expression of ICOSL was observed on all uninfected (mock or GFP-) cells, the surface reduction of this molecule in MCMV infected BMMs and BMDCs was significant (Figure 1B). Similar results were also obtained upon infection of the macrophage cell line IC-21, the dendritic cell line DC2.4, and the endothelial cell line SVEC4-10, although the extent of downregulation differed between them (Figure 1B), being quite dramatic on the IC-21 and DC2.4 cells, and more subtle in the SVEC4-10. Altogether, these findings

demonstrate that MCMV infection causes a consistent and specific downmodulation of ICOSL from the surface of APCs.

We then assessed whether *de novo* viral protein synthesis was required for ICOSL downregulation. To this end, peritoneal macrophages were infected for 72 h (infection rates, approximately 90%) with UV-inactivated MCMV, and the results showed no loss of ICOSL surface expression (Figure 1C), indicating that a productive MCMV infection was required to alter ICOSL expression. To determine the kinetics of ICOSL downmodulation, we examined its surface expression levels at different time points following infection of peritoneal macrophages with MCMV-GFP. As shown in Figure 1D, by 4 hours post infection (hpi) the density of ICOSL at the cell surface was substantially reduced, and by 6 hpi there was barely any ICOSL at the surface of infected cells. When a similar kinetics was conducted in BMDC and IC-21 cells, the downregulation of ICOSL differed with respect to timing, beginning to be evident by 8 hpi and 16 hpi, respectively, with the effect becoming more prominent from that time point onwards. Thus, we concluded that MCMV encodes one or more proteins to rapidly lower cell surface levels of ICOSL upon infection of APCs.

The MCMV m138 gene is responsible for ICOSL downmodulation

In order to find the viral gene/s mediating the observed effects on ICOSL expression, we screened a panel of GFP-expressing MCMV deletion mutants that lack different regions of the viral genome, and which covered a large number of genes dispensable for viral replication in cell culture. The levels of ICOSL were monitored by flow cytometry three days after infection of IC-21 cells with the different mutants. We found that, except for the deletion mutant MCMVΔm128-138, all MCMV mutants tested resulted in the marked downmodulation of ICOSL expression (Figure 2A; see as an example

151 results for the MCMVΔm1-17 mutant). The viral region deleted in MCMVΔm128-138,
152 expanding from ORF m128 to m138, includes some ORFs with functions still
153 unassigned and others involved in viral-host interactions, such as the m129/m131
154 chemokine homolog associated with tropism to macrophages (Fleming et al., 1999;
155 Stahl et al., 2015), or the m138 protein, originally described as an Fc receptor (Thäle et
156 al., 1994), and later reported to be also implicated in the reduction of cell surface
157 expression of the NKG2D ligands H60, MULT-1, and RAE-1ε (Arapović et al., 2009;
158 Lenac et al., 2006), and interestingly, of the co-stimulatory molecule CD80 (Mintern et
159 al., 2006), a member of the B7 family to which also ICOSL belongs. Based on this later
160 feature of m138 and the fact that the viral protein is expressed early during infection, we
161 speculated that the gene altering ICOSL expression in MCMV infected cells might be
162 m138. To directly test the hypothesis, we used an MCMV with a deletion in this gene
163 (MCMVΔm138). As illustrated in Figure 2B, during infection of IC-21 cells with
164 MCMVΔm138, cell surface expression of ICOSL was maintained to levels similar to
165 mock-infected cells, while the levels of CD84, a molecule targeted by the MCMV m154
166 protein (Strazic et al., 2020), used as a control markedly decreased. These effects were
167 not due to a growth defect of the mutant virus in IC-21 cells, as indicated in earlier
168 studies where comparable multi-step growth kinetics between an MCMV deleted in
169 m137-m139 and parental MCMV were observed (Cavanaugh et al., 1996). These results
170 revealed that one gene product, m138, is responsible for the complete downregulation
171 of ICOSL during MCMV infection.
172 We next asked if m138, in the absence of other viral molecules, was sufficient to
173 decrease cell surface levels of ICOSL. To this end, we cloned the m138 gene fused at
174 the C-terminus with the GFP protein and used the resulting recombinant plasmid
175 (named m138-GFP) or the parental GFP only-expressing plasmid (CTL-GFP) to

transiently transfect IC-21 cells. Flow cytometry analysis 24 hours after transfection showed that cells transfected with the m138-expressing construct (GFP+) exhibited a significant reduction of ICOSL surface expression compared to the untransfected control cells from the same cultures or mock-transfected cells (GFP-; Figure 2C, left panel). In contrast, we could not detect any change in the expression of ICOSL in cells transfected with the GFP only-expressing plasmid (compare GFP+ and GFP- cells in Figure 2C, right panel). Therefore, these results indicate that m138 is able to exert its downmodulatory effects on ICOSL expression without requiring the MCMV infection context.

Localization of m138 during MCMV infection

m138 has been predicted to be a 569-aa type I transmembrane glycoprotein (Thäle et al., 1994). Due to the lack of an m138 monoclonal antibody (mAb), the cellular localization of this viral protein during MCMV infection has so far not been directly assessed. Previous studies relied on cells expressing the m138 protein in isolation, or on the different capacity displayed by cells infected with MCMV or with an MCMV mutant lacking the viral protein to bind Ig. Thus, in order to detect m138 in the infection context, we generated a mAb specific for m138, using 300.19 cells stably transfected with the m138 protein HA-tagged at the N-terminus (HA-m138) as immunogen. Then, NIH3T3 cells were infected with MCMV-GFP, and m138 expression was analyzed by indirect immunofluorescence employing this newly generated mAb. As shown in Figure 3A (panels a-c and g), using permeabilizing conditions, the viral protein was detected in perinuclear compartments and cytoplasmic “large punctate vesicles” in GFP+ infected cells. Similar results were obtained in MCMV-GFP infected DC2.4 cells (Figure 3-figure supplement 1). Therefore, these results were consistent with earlier reports in

transfected cells, showing the m138 protein being mainly expressed in intracellular compartments together with markers of the ER, protein disulfide isomerase-A1 (PDI) and calnexin, in addition with the lysosomal marker LAMP-1 (Mintern et al., 2006; Thäle et al., 1994). In contrast, in non-permeabilized infected cells, the mAb against m138 failed to detect the viral protein at the cell surface (Figure 3A, panels d-f), whereas it could be recognized at this location in the 300.19 cells stably transfected with HA-m138 (Figure 3C, left panels). When analyzed by flow cytometry, though, a dim expression of m138 at the cell surface of infected cells could be observed (Figure 3B). As expected, the viral protein was also strongly recognized at the plasma membrane of the transfected cell when assessed by flow cytometry (Figure 3C, right panel). Finally, to evaluate whether m138 could be found in lysosomes, NIH3T3 cells were infected with MCMVwt for 24 h and stained with LysoTracker Red DND99, a fluorescent marker that labels acidic components and is employed to identify lysosomes. Infected cells were then analyzed by immunofluorescence using the m138 specific mAb under gently permeabilizing conditions (0.02% saponin) to preserve the LysoTracker staining. The results, illustrated in Figure 3D (panels c, and d), indicated that m138 colocalized with lysosomes. Indeed, quantification of the m138/lysosome colocalization, using the Coloc2 plugin from FIJI/ImageJ program, led to Manders colocalization coefficients of M1=0.76 and M2=0.80.

m138 prevents ICOSL molecules from reaching the plasma membrane via targeting to lysosomal degradation

We next sought to study the mechanism by which m138 downregulates ICOSL. Since there are no available antibodies capable to detect murine ICOSL in western blot, we generated an NIH3T3 stable cell line expressing HA-ICOSL. We confirmed by flow

cytometry that upon infection with MCMVwt, or following transient transfection with the plasmid expressing GFP tagged m138, but not after infection with MCMVΔm138, HA-ICOSL levels specifically declined at the plasma membrane of the stable HA-ICOSL expressing cell line (Figure 4A and B). NIH3T3 HA-ICOSL cells were then mock-infected or infected with MCMVwt or MCMVΔm138, lysates prepared and western blots performed to examine total ICOSL protein levels by staining for the HA tag. As shown in Figure 4C, two ICOSL specific bands, with apparent molecular masses of ~ 51 and 70 kDa, were detected in the HA-ICOSL stable cell line as compared to untransfected NIH3T3 cells (compare lanes 1 and 2). Notably, in MCMV infected cell lysates, the 70 kDa band was drastically reduced (lane 4), whereas it was not substantially altered after infection with MCMVΔm138 (lane 5), suggesting that this band corresponds to the mature surface form of ICOSL. Indeed, a mild treatment of the NIH3T3 HA-ICOSL cells with trypsin, which selectively cleaves the ectodomains of molecules at the cell surface, and therefore resulted in the loss of detection of ICOSL when assessed by flow cytometry (Figure 4D), led to the disappearance of the 70 kDa band in the western blot (Figure 4C, lane 3). Further demonstration that the larger ICOSL species corresponded to the one present at the cell surface was obtained from a parallel experiment in which we immunoprecipitated lysates from biotinylated HA-ICOSL transfected cells with the anti-HA mAb (Figure 4E). Thus, m138 was altering the expression of the mature form of ICOSL that reaches the cell surface. In addition, we noted, that the 51 kDa band was more abundantly expressed in the infected samples than in the mock-infected samples (Figure 4C, compare lanes 2 with lanes 4 and 5). The fact that ICOSL was slightly induced at the cell surface after treatment with UV-inactivated MCMV (Figure 1C), could indicate that virion components or the process of viral binding may be causing these effects. Supporting this observation, an analysis of

extracts from NIH3T3 HA-ICOSL cells infected with UV-inactivated MCMV indicated that this was the case, with both the 51 kDa and the 70 kDa bands being considerably more abundant than in the mock-infected samples (Figure 4F, compare lanes 2 and 4). Thus, MCMV infection initially induces ICOSL expression and m138 subsequently leads to the depletion of cell-surface ICOSL, but not of the overall intracellular levels of this molecule.

Taking into account the intracellular localization of m138 and the fact that it targets the B7 costimulatory molecule CD80 early in the secretory pathway, rerouting it to lysosomes, we contemplated the possibility that the viral protein was behaving in a similar way to interfere with ICOSL (Mintern et al., 2006). We addressed this issue by co-transfecting NIH3T3 cells with the plasmid encoding for HA-ICOSL together with either the construct expressing m138-GFP or an unrelated GFP protein (CTL-GFP), and analyzing the levels of ICOSL expression by western blot before and after treatment with a combination of two lysosomal inhibitors, leupeptin and bafilomycin. Under these transient transfection conditions, and in contrast to the assays in stably transfected NIH3T3 HA-ICOSL cells, ICOSL and m138 were simultaneously expressed, without previous existence of ICOSL at the cell surface. As shown in Figure 5A, in cells co-transfected with the m138-GFP protein, independently of whether or not the lysosomal inhibitor treatment was applied, the 70 kDa ICOSL band, corresponding to ICOSL on the cell surface, was not observed (lanes 4 and 5). In addition, the results also evidenced that the 51 kDa band, corresponding to intracellular ICOSL, augmented (1.5-fold) after exposure to leupeptin and bafilomycin (compare lanes 4 and 5). In contrast, in cells expressing the CTL-GFP protein, both the 51 and 70 kDa bands were present, and the blockade of the lysosomal pathway did not lead to a substantial alteration (1.1-fold) of any of the two ICOSL forms (Figure 5A, compare lanes 2 and 3). The presence of the

70 kDa mature form of ICOSL when the CTL-GFP was expressed, and its absence upon expression of m138-GFP under conditions of lysosomal inhibition, pointed out that the viral protein was targeting ICOSL before reaching the cell surface. We then infected NIH3T3 HA-ICOSL cells with MCMVwt and examined by confocal fluorescence microscopy m138 and ICOSL expression. A marked colocalization of ICOSL and the viral protein in perinuclear compartments and in cytoplasmic punctate structures could be observed, being more robust after treatment with the lysosomal inhibitors (Figure 5B, panels g and h). Accordingly, the expression signal of ICOSL was also increased after treatment with leupeptin and bafilomycin (compare panels a and e in Figure 5B). The results also showed augmented levels of m138 upon exposure to the lysosomal inhibitors (compare panels b and f), indicating that m138 was getting partially co-degraded with its target. These observations were confirmed by flow cytometry in permeabilized NIH3T3 HA-ICOSL MCMV-infected cells, where significant higher levels of expression of both ICOSL and m138 could be detected after blockade of the lysosomal pathway (Figure 5C). Collectively, the data suggest that m138 precludes the maturation of ICOSL by targeting it to lysosomes, explaining how the levels of this co-signaling molecule are decreased at the cell surface.

m138 interacts with ICOSL

We then considered the possibility that m138 might be interacting with ICOSL, as it has been previously shown for CD80. To this end, we performed coimmunoprecipitation assays using NIH3T3 cells transiently expressing m138-GFP and HA-ICOSL. Proteins were pulled down by an anti-HA antibody and analyzed by western blot using an antibody against GFP. Taking into account the potential capacity of m138 to bind IgG, an immunoprecipitation was carried out with an anti-human Fc antibody as a control.

As illustrated in Figure 5D, the m138 protein was recovered when the immunoprecipitation was carried out with the anti-HA antibody (lane 2), whereas when using the antibody against human Fc the viral protein was not detected (lane 1). As expected, after stripping the western blot and reprobing it with an anti-HA antibody, the 51 kDa specific ICOSL band was only observed in the precipitates obtained from the anti-HA mAb pull downs. These data suggest that m138, either directly or in an indirect manner, associates with ICOSL.

Distinct m138 structural domains are required to downmodulate the two members of the B7 family, ICOSL and CD80

The ectodomain of m138 is predicted to be composed by three Ig-like domains (Lenac et al., 2006; Corrales -Aguilar et al., 2014). Previous work using mutant MCMVs containing m138 versions defective in either three potential Ig-like domains indicated different structural requirements in this viral protein for the downregulation of the NKG2D ligands (Lenac et al., 2006). We investigated if this was also the case for m138 to exert its effects on the two co-stimulatory molecules ICOSL and CD80, since this could allow us to dissect the impact of the viral protein on the two pathways of T-cell activation. Thus, we created three different m138-GFP mutants, missing the putative N-terminal Ig domain (Ig1; m138ΔIg1-GFP), the middle Ig domain (Ig2; m138ΔIg2-GFP), or both the middle and membrane-proximal (Ig3) Ig domains (m138ΔIg2/3-GFP) (Figure 6A, schematic representation of these constructs). Each m138-GFP mutant construct was transiently expressed on NIH3T3 HA-ICOSL cells and surface levels of ICOSL and CD80 were assessed by flow cytometry and compared to those present in cells transfected with the m138-GFP control. As shown in Figure 6B, the m138ΔIg1-GFP protein was incapable to significantly reduce ICOSL or CD80 cell surface levels.

In contrast, while CD80 surface density decreased in cells transfected with m138ΔIg2-GFP and m138ΔIg2/3-GFP, these two m138 mutants did not alter in a substantial manner ICOSL expression. Therefore, we conclude that the Ig1 domain of m138 is absolutely required for both ICOSL and CD80 downregulation. However, while the putative Ig2 and Ig3 domains of m138 need to be preserved for the downregulation of ICOSL, they are dispensable for m138-mediated decrease of CD80 expression.

m138 curtails ICOSL-dependent antigen presentation and subsequent $CD8^+$ T-cell responses during MCMV infection of APCs

The differential structural requirements of m138 to target CD80 and ICOSL permitted us to specifically address the functional consequences of the disruption of the ICOSL:ICOS pathway during the course of the MCMV infection. To this end, we employed two MCMV mutants containing m138 versions lacking either the Ig2 domain (MCMVm138ΔIg2), or the Ig2 and Ig3 domains (MCMVm138ΔIg2/Ig3). As it occurred in transfection assays with the m138 mutant plasmids defective in these Ig domains, infections with MCMVm138ΔIg2 or MCMVm138ΔIg2/Ig3 led to decreased cell-surface density of CD80 but not ICOSL (Figure 7A). We then performed an *in vitro* antigen presentation assay assessing the effect of these two MCMV mutants on the ability of APCs to induce an ICOSL-dependent $CD8^+$ T-cell response, in comparison to that of MCMVwt and MCMVΔm138. We co-cultivated BMDCs infected with the different viruses with naive $CD8^+$ T cells from splenocytes derived from T-cell receptor (TCR)-transgenic mouse line in which 90% of $CD8^+$ T-cells are specific for MCMV M38 peptide, and measured the percentage of IFN-γ^+ $CD8^+$ T cells 6 h later (Figure 7B, schematic model) (Maxi mice; Torti et al., 2011). Remarkably, as illustrated in Figure 7B, both MCMVm138ΔIg2 and MCMVm138ΔIg2/Ig3-infected BMDCs stimulated

significantly stronger IFN-γ responses by $CD8^+$ T cells as compared to the MCMVwt infected cells. Moreover, the magnitude of the IFN-γ induction observed with these two MCMV mutants, which downregulated CD80 but preserved cell surface levels of ICOSL intact, almost approached the levels obtained in MCMVΔm138-infected BDMCs. These findings provide evidence for a substantial contribution of the m138 protein in the evasion of the $CD8^+$ T-cell immune response via manipulation of the ICOSL:ICOS axis (Figure 7B).

m138 impairs ICOS-dependent T-cell responses *in vivo* and limits virus control

We then explored the relevance of ICOSL interference by m138 during the acute MCMV infection. First, we sought to confirm that ICOSL downmodulation by MCMV was taking place in the *in vivo* context. Adult BALB/c mice were intraperitoneally (i.p.) infected with $2x10^6$ PFU of MCMV-GFP, and 48 h later the levels of ICOSL were analyzed in peritoneal macrophages by flow cytometry. As shown in Figure 8A, we observed a significant reduction of ICOSL levels, in parallel to those of MHC I used as a positive control, on the surface of the GFP+ MCMV-infected as compared to the uninfected GFP- macrophages. In addition, we directly assessed whether ICOSL was being specifically downregulated by m138 on peritoneal DCs during the *in vivo* infection. Thus, BALB/c mice were mock-infected or i.p. infected with $1x10^6$ PFU of MCMVwt or MCMVΔm138, and at 6 hpi cell surface levels of ICOSL and CD80 were determined by flow cytometry on infected peritoneal DCs (positive for the MCMV protein m04) and compared to those on peritoneal DCs derived from mock-infected mice. Figure 8B illustrates a marked MCMVwt-induced downmodulation of ICOSL on peritoneal DCs, and a subsequent significant augmentation of the levels of this molecule in the absence of m138, on the surface of MCMVΔm138-infected peritoneal DCs. In the

case of CD80, although the downmodulation caused by MCMVwt was subtle, a clear increase of CD80 levels was detected on MCMVΔm138-infected cells when compared to both mock-infected and MCMVwt-infected DCs. Therefore, these results confirmed a role of m138 downmodulating ICOSL and CD80 on primary mouse DCs (Figure 8B).

It has been previously described that the MCMV mutant depleted of m138 is attenuated early after infection in an NK-dependent manner, attributing this phenotype to the already reported activities of this viral protein downregulating NKG2D ligands (Lenac et al., 2006). Taking in consideration m138 effects on the two co-stimulatory molecules CD80 and ICOSL, we sought to assess the contribution of m138 at later times of the acute infection by comparing the *in vivo* phenotype of MCMVm138ΔIg2 with that of MCMVΔm138 and MCMVwt under conditions that included depletion of NK cells or combined depletion of NK cells and $CD4^+$ and $CD8^+$ T cells. Of note, previous work with MCMVm138ΔIg2 showed that this mutant virus was capable to downregulate NKG2D ligands MULT-1 and RAE-1ε, but not H60 cell surface molecules (Arapović et al., 2009; Lenac et al., 2006). The information of the effects that MCMVwt and mutants have on these m138 targeted host molecules on the surface of infected cells is indicated in part C of Figure 8. C57BL/6 mice were intravenously (i.v.) infected with $2x10^5$ PFU of the different viruses, left untreated or treated with the antibodies to deplete specific lymphocyte subsets, and viral titers in salivary glands and lungs were quantified 14 days post infection (dpi) (Figure 8D, schematic representation of the assay). As illustrated in Figure 8D, in the salivary glands, viral titers of MCMVm138ΔIg2, a mutant which is unable to downregulate H60 and ICOSL, were lower than those of MCMVwt. In fact, the MCMVm138ΔIg2 titers in this organ were below the detection limits for all animals, in a similar way as in MCMVΔm138 infected mice. NK cell depletion led to a substantial increase of both MCMVΔm138 and MCMVm138ΔIg2 infection in this

organ, but importantly, MCMVm138ΔIg2, which was downmodulating CD80 but not ICOSL, was still heavily attenuated as compared to MCMVwt under these conditions. This finding indicated that ICOSL targeting by m138 is important for the virus to increase its load in salivary glands. Conversely, the downregulation of CD80 by m138 did not seem to play a major role during MCMV replication in this organ. Furthermore, when besides NK cells, $CD4^+$ and $CD8^+$ T cells were depleted, MCMVm138ΔIg2 growth in the salivary glands was completely restored, indicating that m138 via interference with ICOSL evades T-cell responses. It is important to note that when NK cells together with $CD4^+$ and $CD8^+$ T cells were depleted, MCMVΔm138 seemed to be slightly attenuated. This may suggest that m138 is capable to perform additional immune evasion activities independent of NK and T cells. Similar results were obtained when viral titers were evaluated in the lungs of the infected animals, although in this case the contribution of m138 via ICOSL in the control of the MCMV infection seemed to be less significant (Figure 8D).

MCMV has been reported to induce the accumulation of virus-specific $IL10^+$ $CD4^+$ T cells in an ICOSL-dependent manner in salivary glands (Clement et al., 2016). Thus, we directly addressed the impact of m138 on the evasion of MCMV-specific $CD4^+$ T cells responses in various organs. To this end, we adoptively transferred TCR-transgenic $CD4^+$ T cells specific for the M25 protein (M25-II; Mandaric et al., 2012) into C57BL/6 SCID mice, depleted them of NK cells, and one day later infected them with $2x10^5$ PFU of MCMVwt or MCMVΔm138 (See schematic model in Figure 8-figure supplement 1). Seven days after infection, the expansion of $CD4^+$ T cells was determined in the spleen, lungs and salivary glands. The data, illustrated in Figure 8-figure supplement 1, show that the frequencies of $CD4^+$ T cells increased in the three organs analyzed upon MCMV infection. Moreover, a role of the viral m138 protein participating in immune

426 evasion of $CD4^+$ T cells could be observed in spleen and lungs when comparing data
427 from MCMVwt and MCMVΔm138 infections, although this was not the case in the
428 salivary glands.
429
430 **The ICOSL:ICOS axis contributes to the generation of MCMV-specific humoral**
431 **immune responses *in vivo***
432 We also sought to determine the importance of ICOSL-mediated co-stimulation for
433 mounting MCMV-specific T-dependent antibody responses. We approached this, by
434 inhibiting ICOSL:ICOS interaction during the acute MCMVΔm138 infection via the
435 administration of a blocking anti-ICOSL antibody. Groups of BALB/c mice were
436 infected with $2x10^6$ PFU of MCMVΔm138 and treated with or without an anti-ICOSL
437 mAb, starting one day prior infection. Salivary gland draining lymph nodes and spleens
438 were extracted in order to analyze by flow cytometry different T and B lymphocyte
439 subsets, and blood collected, at day 14 post infection. As illustrated in Figure 9A, a
440 marked decrease of the percentage of Tfh cells in both spleen and lymph nodes was
441 observed when infected mice were deprived of ICOSL-mediated signals. In addition,
442 while the percentage of follicular B cells was not substantially altered, or was even
443 slightly higher, upon ICOSL blockade, GC B cells in lymph nodes were dramatically
444 reduced. Consistent with these observations, an analysis by immunofluorescence of
445 splenic sections revealed that GCs were smaller in size in the infected mice that
446 received anti-ICOSL antibody as compared to mice that did not received it, whereas this
447 was not the case of the follicles, whose sizes seemed not to be affected by the treatment
448 (Figure 9B). These results, which are in agreement with the phenotype associated with
449 ICOS absence, pointed to a disturbed production of MCMV specific antibodies during
450 the primary infection under conditions of ICOSL blockade. No significant differences in

451 the percentage of other cell subsets such as marginal zone B cells, B1 B cell subsets,
452 plasma cells, or overall $CD4^+$ and $CD8^+$ T cells between the two groups of infected
453 animals were detected (Figure 9-figure supplement 1). In addition, the blockade of
454 ICOSL also resulted in an increased percentage of naïve $CD4^+$ T cells in the spleen and
455 decreased percentages of memory $CD4^+$ T cells in spleens and lymph nodes (Figure
456 9A), an indication that long lasting immune protection to MCMV could be also
457 impaired in the absence of ICOSL:ICOS signaling.
458 Due to the above results and the implication of ICOS in promoting T-dependent
459 antibody responses, we assessed by ELISA whether the levels of MCMV-specific
460 antibodies in the sera of the infected mice were altered after ICOSL blockade. We
461 observed that mice that received the anti-ICOSL antibody had significantly reduced
462 levels of total IgG specific for MCMV than those that did not receive it (Figure 10A).
463 When we evaluated the serum levels of the predominant subclasses of natural
464 antibodies, a substantial decreased production of MCMV-specific IgG1 and IgG2a and
465 b was detected in infected animals in which ICOSL was blocked, while no differences
466 were found in the production of MCMV-specific IgG3 or IgM responses between both
467 groups (Figure 10A). These results indicated that ICOSL-mediated co-stimulation was
468 crucial for the development of MCMV-specific IgG1 and IgG2 responses.
469 The observed alterations in the humoral responses prompted us to conduct *in vitro*
470 neutralization assays of MCMV with the serum of the infected mice. As illustrated in
471 Figure 10B, sera from mice that received the anti-ICOSL antibody exhibited a
472 significant lower capacity to neutralize MCMV compared to those that did not received
473 it. Similar findings were obtained when the neutralization assays were performed in the
474 presence of complement (Figure 10-figure supplement 1). In conclusion, our findings

indicate a prominent role of ICOSL:ICOS interactions in the induction of effective T and B cell responses during MCMV infection.

HCMV reduces cell surface levels of ICOSL on APCs

We then investigated if HCMV has also the capacity to interfere with cell surface expression of ICOSL in APCs. To this end, human primary monocyte-derived macrophages were infected with HCMV-GFP (TB40/E strain), and analyzed by flow cytometry 72 hours after infection. In addition, we tested the viral effects on the THP-1 cell line differentiated by treatment with the protein kinase-C agonist phorbol-12-myristate-13-acetate (PMA). As shown in Figure 11A, in both cell types, HCMV infection resulted in a marked reduction in cell surface ICOSL expression compared to non-infected cells in the same culture or to mock-infected cells. In contrast, cell surface expression of CD70 remained unaffected, indicating that ICOSL molecules were specifically targeted in HCMV infected cells. Kinetic assays performed in THP-1 cells indicated that by 24 hpi ICOSL levels were already drastically reduced (Figure 11B). As shown in Figure 11C, the fact that upon infection with UV-inactivated HCMV ICOSL density at the plasma membrane was not significantly different from that of mock-infected control cells, suggested that the expression of one or more viral gene products were required to downmodulate ICOSL. We also analyzed whether the total levels of ICOSL were altered upon infection, by carrying out immunoblot analysis on uninfected or HCMV infected protein lysates using an anti-ICOSL polyclonal antibody. As can be seen in Figure 11D, ICOSL in the THP-1 uninfected cells migrated as a broad band of approximately 70 kDa. In contrast, after infection with HCMV, the levels of ICOSL were drastically reduced. Interestingly, we observed that treatment with leupeptin and bafilomycin was not able to significantly restore ICOSL expression.

500

501 **Additional herpesviruses also target cell surface ICOSL**

502 Finally, we asked whether, similar to murine and human CMVs, other human
503 herpesviruses are also able to alter ICOSL cell-surface expression during the course of
504 the infection. We focused on HSV-1 and HSV-2, and infected THP-1 cells using GFP
505 versions of these viruses. Notably, as illustrated in Figure 11E, the levels of ICOSL
506 were reduced during infection of both HSV-1-GFP and HSV-2-GFP compared to those
507 of or mock-infected cells. In contrast, surface expression of CD70 did not change,
508 confirming the specificity of the findings. Moreover, the observation that upon infection
509 of THP-1 cells with UV-inactivated HSV-1 and HSV-2, only a partial downregulation
510 of ICOSL was observed, indicated that these two human viruses also harbor genes
511 targeting ICOSL (Figure 11E). Last, when we evaluated by western blot ICOSL
512 expression in whole THP-1 cell lysates, a clear reduction of the levels of this molecule
513 could be appreciated upon infection with both HSV-1 and HSV-2 (Figure 11F).
514 Altogether, these findings demonstrate that ICOSL downregulation is a strategy used by
515 different herpesviruses.

Discussion

Co-stimulatory molecules play a decisive role in shaping the extent and nature of the cell-mediated adaptive immune response by tuning T-cell activation. Therefore, it is not surprising that pathogens, including viruses, have devised mechanisms to abrogate their signaling and blunt host responses that would otherwise limit their replication (Khan et al., 2012). In this study, we demonstrate that the ligand for the co-stimulatory molecule ICOS is dramatically diminished from the surface of APCs during infection by different herpesviruses. With a primary focus on MCMV, the most widely used model to study CMV infection, we show that the downregulation of ICOSL restricts the magnitude of MCMV-specific T-cell responses and potentiates viral burden *in vivo.*

We describe here that ICOSL expression is slightly induced upon cell exposure to MCMV, presumably due to viral sensing by pattern recognition receptors. However, MCMV rapidly removes this molecule from the surface of infected cells by expressing m138. Infections with an MCMV lacking the *m138* gene, and assays with the viral gene expressed in isolation, indicate that m138 is necessary and sufficient to decrease ICOSL cell surface levels. The early-expressed m138 protein, which is an Fc receptor homologue, has been shown not only to bind the constant Fc domain of IgG, but also to downmodulate the expression of three cellular ligands of the activating NKG2D receptor, RAE-1ε, H60, and MULT-1, and another B7 family molecule, CD80 (Arapović et al., 2009; Lenac et al., 2006; Mintern et al., 2006; Thäle et al., 1994). Consequently, this viral protein holds the potential to control the antiviral function of NK and T cells, as well as the humoral response. Hence, the m138 early glycoprotein provides an excellent example of how CMVs have refined proteins to execute multiple immune-evasion functions. It is becoming increasingly clear that the evolution of

multifunctional proteins is not only a hallmark of RNA viruses, with limited genome sizes and relatively small number of genes, but that it is also employed by large DNA viruses to make optimal use of their coding capacity. For instance, MCMV produces the multifaceted immunomodulatory protein m152, which is capable of downregulating MHC class I molecules and different RAE-1 isoforms, as well as modulating the cGAS-STING pathway, thereby evading type I IFN-, NK- and T cell-dependent immune responses to MCMV infection (Fink et al., 2013; Krmpotić et al., 1999; Lodoen et al., 2003; Stempel et al., 2019; Ziegler et al., 1997). Moreover, we have recently demonstrated that by interfering with AP-1 mediated protein sorting, the m154 glycoprotein targets a broad-spectrum of cell surface molecules implicated in the antiviral NK and T-cell responses (Strazic et al., 2020; Zarama et al., 2014). In HCMV, this concept is best exemplified by the *US12* family, whose members, as it will be discussed below, have been reported to alter the expression of numerous plasma membrane proteins, mainly NK ligands, adhesion proteins and cytokine receptors (Fielding et al., 2017).

m138 is a 69 kDa type I transmembrane glycoprotein, largely localized in the ER and lysosomal compartments, and shown to be further processed into a 105 kDa highly glycosylated form (Mintern et al., 2006). Based on the ability of MCMV infected cells to bind IgG, m138 was reported to be a cell surface resident protein, a feature shared by the different viral Fcγ receptors (Corrales-Aguilar et al., 2014; Lenac et al., 2006). Consistent with its location at the plasma membrane, the viral protein was shown to perturb the endocytosis of surface RAE-1ε and MULT-1, interfering with the clathrin dependent endocytosis of this later cellular target, altering its recycling and leading to its subsequent degradation in lysosomes (Arapović et al., 2009; Lenac et al., 2006). A

different mode of action was reported for m138 in the downregulation of CD80, targeting the cellular molecule when newly synthesized early in the secretory pathway and mislocalizing it to lysosomal compartments (Mintern et al., 2006). To date, studies on the maturation and posttranslational modifications of ICOSL are still lacking, but our observations are compatible with the notion that, as in the case of CD80, m138 interacts with ICOSL, preventing it to mature and reach the plasma membrane, and driving this molecule to lysosomal degradation. Accordingly, we found that during MCMV infection, m138 and ICOSL colocalize in intracellular compartments, where the viral protein is primarily expressed, and that upon treatment with lysosomal inhibitors the levels of both ICOSL and m138 augment. Moreover, our co-precipitation experiments demonstrate that indeed m138 directly associates with ICOSL. The details on how the interactions of m138 with its structurally diverse targets can potentially occur remain to be elucidated. In this regard, solving the crystal structure of m138 alone or bound to its cellular targets may be of great value for understanding its versatility and different modes of action.

Due to the multiple cellular targets of m138, dissecting the functional consequences of lessening ICOSL cell surface levels on virally infected cells appeared to be complicated. m138 was predicted to contain an ectodomain with three putative Ig-like domains, exhibiting a relatively low but yet significant sequence homology with the Ig-like domains of murine FcγRs CD16 and CD32 (Budt et al., 2004; Lenac et al., 2006). Previous work indicated distinct m138 structural requirements to downmodulate the different NKG2D ligands (Arapović et al., 2009; Lenac et al., 2006; Mintern et al., 2006). Thus, by generating versions of the m138 protein devoid of some of its Ig domains, and through the use of MCMV recombinants bearing similar deletions within

591 the viral protein, we determined that the downregulation of the two B7-molecules,
592 ICOSL and CD80, was dependent on the N-terminal m138 Ig domain. However, while
593 the middle and membrane-proximal Ig domains of m138 were largely dispensable for
594 disturbing CD80, they needed to be preserved for ICOSL cell surface removal. This
595 result indicates a distinct mode of action of m138 to target the two costimulatory
596 molecules, and gave us the opportunity to separate the corresponding impacts on T-cell
597 activation. Optimal T-cell activation is characterized by rapid proliferation, cytokine
598 production and efficient effector functions. Importantly, employing an *in vitro* antigen
599 presentation assay and the m138 mutant MCMVs, we showed that via ICOSL
600 downmodulation, m138 contributes to impair antiviral $CD8^+$ T-cell responses. This
601 agrees with the earlier evidence that the m138 protein expressed in isolation is capable
602 to reduce the ability of DCs to promote T-cell activation in a CD80-dependent manner,
603 and the fact that applying a blocking anti-CD80 antibody only partially reverted these
604 effects (Mintern et al., 2006). Our observations, however, in the context of the infection,
605 point to a prominent role of the ICOSL-dependent m138 function compromising T-cell
606 stimulation. The m138 protein has not an ortholog in HCMV. However, we demonstrate
607 that following a productive HCMV infection of primary monocyte-derived
608 macrophages or differentiated THP-1 cells, which express high levels of ICOSL, a
609 strong ICOSL cell surface downregulation also takes place, and that this process
610 requires viral gene expression. Using a multiplexed proteomic approach and HCMVs
611 with deletions of each individual ORF of the *US12* viral family, Fielding and co-
612 workers had previously described that members of this family selectively target a
613 number of plasma membrane proteins crucial for NK cell activity, adhesion, and
614 cytokine signaling during HCMV infection of human fibroblasts (Fielding et al., 2017).
615 Interestingly, in these assays, and despite the low levels of ICOSL in human fibroblasts,

no reduction of cell surface ICOSL could be observed after infection with HCMVs deleted in either US16 or US20, strongly suggesting that these two HCMV products are involved in ICOSL downregulation. Our findings also indicate that HCMV not only leads to diminished cell surface ICOSL, but also to an abrogation of its expression in whole cell levels, via a lysosomal degradation-independent process. Importantly, a similar complete loss of ICOSL on differentiated THP-1 cells was observed during infection by two α-herpesviruses, HSV-1 and HSV-2. In this case, though, both the mechanism as well as the identity of the viral proteins involved in this process remain to be defined.

The importance of the ICOSL:ICOS pathway has been explored in several models of bacterial and parasitic infections (Wikenheiser and Stumhofer, 2016). However, to date, only a limited number of studies on murine models of infection with RNA viruses (LCMV, VSV, and influenza virus), in conditions of ICOS deficiency or blockade with an ICOSL-Ig molecule, have been reported, and shown that ICOS triggering plays a marginal although significant role in the development of $CD4^+$ T-cell effector responses (Bertram et al., 2002; Kopf et al., 2000). But, persisting DNA viruses, with infections more dependent on cell-mediated immune control, may differ. Besides the role played by ICOS in directing effector T-cell activation, proliferation and differentiation, this molecule has been crucially implicated in the generation of T-dependent antibody responses. Thus, in this study we examined whether anti-MCMV humoral immune responses were altered in the absence of ICOS signaling. Overall, our data employing a blocking monoclonal anti-ICOSL antibody in the context of the acute MCMV infection revealed a high importance of the ICOSL:ICOS axis in the formation of Tfh cells and subsequent GC B-cell development in spleens and lymph nodes follicles, consistent

with what has been previously observed in other *in vivo* experimental models of infection (Wikenheiser and Stumhofer, 2016). Importantly, as a consequence of the observed effects, ICOSL blockade was associated with a lower production of MCMV-specific IgG1 and IgG2 antibodies. Furthermore, a decreased capacity of the antibodies generated to neutralize MCMV was also observed. Notably, while the CD80/CD86:CD28 co-stimulatory pathway has been shown to be also involved in the induction of Tfh cells and class switching of MCMV-specific antibodies, we find that this pathway is not capable to compensate the defects observed in the absence of ICOS signaling, evidencing the non-redundant role of the two axis in this scenario (Welten et al., 2016). We have not directly addressed here whether the lack of ICOSL co-stimulation is associated with a deficient viral control, due to the highly attenuated phenotype of the MCMV defective in m138 employed in the study. Remarkably, a reduction of splenic $CD4^+$ memory T cells was also observed in our assays upon ICOSL blockade, further supporting the potential significance of the ICOSL:ICOS axis in the long term protection against MCMV. Of interest, ICOS- and ICOSL-deficient patients have been associated with combined T- and B-cell immunodeficiency, and importantly, with an increased susceptibility to viral infections (Roussel et al., 2019; Schepp et al., 2017). Moreover, while the infectious phenotype of these patients varied, a high incidence of recurrent herpesvirus infections, mostly including herpes simplex and cytomegalovirus infections, was observed.

It was previously shown that deletion of m138 or both m138 and the CD86 downmodulator m147.5 from MCMV has a dramatic impact on viral load during acute infection (Arens et al., 2011; Crnković-Mertens et al., 1998). To directly address the potential importance of m138-mediated downregulation of ICOSL on viral growth *in*

vivo we employed the recombinant MCMV expressing m138 without the middle Ig domain, and therefore able to downmodulate CD80 and CD86 but not ICOSL in infected APCs. The fact that under conditions of NK cell depletion the viral mutant was still attenuated at late times post infection, particularly in the salivary glands, and the nearly complete reversion of this defective phenotype in the absence of NK cells and T cells, indicated that m138 by interfering with ICOSL contributes to subvert T-cell responses *in vivo*. By performing adoptive transfer assays of exogenous M25-specific transgenic $CD4^+$ T cells into C57BL/6 SCID mice, which were depleted of NK cells, and infected with MCMVwt or the MCMV lacking m138, we evaluated the impact that the viral protein may have on immune evasion of $CD4^+$ T cells in various organs. We observed that m138 clearly contributes to diminish M25-specific $CD4^+$ T cell proliferation in spleen and lungs of infected mice, but not in salivary glands, where virus specific $CD4^+$ T cells are important for control of the viral infection. It must be noted, however, that since in the study we only measured M25-specific responses, we cannot discard that in the salivary glands m138 may be influencing in a different way $CD4^+$ T cell responses specific for other MCMV epitopes. Altogether, our results support the notion that downmodulation of ICOSL by m138 represents an effective immune evasion strategy during the acute MCMV infection. Taking in account these observations, an aspect that deserves to be explored is whether these ICOSL-related activities can be employed by additional herpesviruses or other viral pathogens as a mean to escape host immune surveillance.

In conclusion, in this study we present a novel viral tactic to impair T-cell activation, based on the interference with the ICOS:ICOSL co-stimulation pathway. To this end, the herpesviruses analyzed so far seem to exploit “self” proteins, evolved during co-

691 evolution with their hosts, being in the case of murine CMV, a multitasking
692 immunoevasin. Ultimately, the study of these immunoevasin should provide not only
693 new insights into viral pathogenesis, but also enlighten us about critical biological and
694 immunological processes that promote viral control.

Material and methods

Ethics statement

All procedures involving animals and their care were approved (protocol number CEEA 308/12) by the Ethics Committee of the University of Barcelona (Spain) and the Animal Welfare Committee at the University of Rijeka (Croatia) and were conducted in compliance with institutional guidelines as well as with national (Generalitat de Catalunya decree 214/1997, DOGC 2450) and international (Guide for the Care and Use of Laboratory Animals, National Institutes of Health, 85–23, 1985) laws and policies. Human blood was obtained from healthy volunteer donors through the Blood and Tissue Bank of the Catalan Department of Health (Barcelona, Spain). Utilization of blood products for the experiments conducted was approved by the Ethics Committee of the Hospital Clinic of Barcelona (Barcelona, Spain), and according to the principles of the Declaration of Helsinki.

Cell cultures

NIH3T3 (mouse embryonic fibroblasts), SVEC4-10 (SV40-transformed mouse endothelial cells), HFF (human foreskin fibroblasts), HEL299 (human embryonic lung fibroblasts), MEFs (primary mouse embryonic fibroblasts), MEFs immortalized with p53 (kindly provided by Dr. Jay Nelson [Oregon Health Sciences University, Portland, USA]), and Vero cells were cultivated in Dulbecco's modified Eagle's medium (DMEM) supplemented with 2 mM glutamine, 1 mM sodium pyruvate, 50 U/mL of penicillin, 50 g/mL of streptomycin, and 10% fetal bovine serum (FBS). IC-21 (mouse peritoneal macrophages transformed with SV-40), DC2.4 (mouse dendritic), NS1 (mouse myeloma), THP-1 (human monocytic) and 300.19 (mouse pre-B) cells were

cultured in RPMI-1640 medium, supplemented as indicated above, and for THP-1 and 300.19 cells, 0.05 mM 2-mercaptoethanol was added. Primary mouse peritoneal macrophages were elicited from peritoneal exudate cells from BALB/c mice receiving 1 mL of thioglycolate i.p. 4 days before the extraction. Primary peritoneal dendritic cells were isolated according to Ray and Dittel (2010). Splenocytes and lymph nodes obtained from mice were subjected to a manual disaggregation and treatment with red blood cell lysis buffer (0.15 M NH4Cl, 0.01 M Tris HCL) to obtain cell suspensions. Primary mouse dendritic cells and macrophages from bone marrow of femur bones from BALB/c mice or C57BL/6 were obtained after 7 days of culture in RPMI-1640 medium supplemented as indicated above, with the addition of granulocyte-macrophage colony-stimulating factor (GM-CSF) at days 3 and 6 from extraction. Attached cells were enriched in macrophages whereas suspension fractions were enriched in dendritic cells. Both type of cells were plated in flat-bottom 24-well dishes with the supplemented RPMI-1640 medium at a concentration of $2x10^5$ cells/well. Dendritic and macrophage differentiation were confirmed by flow cytometry using the markers CD11c and, F4/80, respectively. Primary human monocytes were obtained from PBMCs isolated by Ficoll-Paque density-gradient centrifugation from fresh blood samples of human healthy donors. Monocyte-derived macrophages (MDM) were differentiated after culturing monocytes for 5 days in RPMI-1640 medium supplemented as indicated for mouse primary cells, with 50 ng/mL of GM-CSF. Cell lines were routinely tested for mycoplasma contamination with MycoAlert Mycoplasma Detection Kit from Lonza.

Viruses and infections

744 The bacterial artificial chromosome (BAC)-derived MCMV strain MW97.01, here
745 referred as MCMVwt (Wagner et al., 1999), and the MCMV-GFP recombinant virus, a
746 derivative of MW97.01 carrying the GFP gene (Mathys et al., 2003), were used as
747 parental viruses throughout the study. Recombinant strains MCMV-GFPΔ15 lacking
748 genes from *m128* to *m138* (termed here MCMV-GFPΔm128-m138) and MCMVΔm138
749 lacking the *m138* gene, have been described previously (Lenac et al., 2006), as well as
750 recombinant strain MCMV-GFPΔ1 lacking genes from *m1* to *m17* (termed here
751 MCMV-GFPΔm1-m17; Brune et al., 2006). MCMV mutants containing m138 versions
752 without Ig2 domain (MCMVm138ΔIg2), or without Ig2 and Ig3 domains
753 (MCMVm138ΔIg2/Ig3) were also described in Lenac et al., 2006. Viral stocks were
754 grown by infecting MEFs cells at a low moi using DMEM supplemented as stated
755 above, except that 3% FBS was used. Cell supernatants were recovered when maximum
756 cytopathic effect was reached, and cleared of cellular debris by centrifugation at 1750 g
757 for 10 min. The HCMV strain TB40/E carrying the *GFP* gene was used in the study
758 (termed here HCMV-GFP; Sinzger et al., 2008). HCMV stocks were prepared as
759 indicated for MCMVs, but using in this case HEL299 or HFF cells. HSV-1 and HSV-2
760 containing the GFP gene were kindly provided by Dr. Antonio Alcamí (Autonomous
761 University of Madrid, Spain). Both viruses were grown in Vero cells. Viral titers were
762 determined by standard plaque assay on primary BALB/c MEFs, MEFs p53, HEL299
763 or Vero cells for MCMV, HCMV, or HSV-1 and HSV-2, respectively. Infections of
764 murine peritoneal macrophages, bone marrow dendritic cells and IC-21 cells included a
765 centrifugal enhancement of infectivity step (Hudson, 1988). C57BL/6 derived DCs were
766 infected by incubating cells in suspension with the virus for 30 min in a small volume
767 ($c=10^7$ cells/mL) with occasional agitation at 37ºC. THP-1 cells were activated for 24 h
768 with 50 ng/mL PMA (Sigma-Aldrich) prior the infection. THP-1 cells and MDM were

infected in the presence of PMA or GM-CSF, respectively, for 16 hours, and also included a step of centrifugal enhancement of infectivity. UV-inactivation of virus was performed using a UV crosslinker (HL 2000 hybrilinker) for 3 min at 360 mJ/cm^2.

Antibodies

For flow cytometry analysis we used the following anti-mouse antibodies: ICOSL-biotin or ICOSL-PE (clone HK5.3), MHCI-PE (clone M1/42), B7.1-APC (clone 16-10A1), CD84-PE (clone mCD84.7), CD11c-A647 or -APC (clone N418), F4/80-PE (clone BM8), B220-PB (clone RAE-6B2), CD5-PE (clone 53-7.3), CD138-PECy7 (clone 281-2), CD3-A488 (clone 17A2), CD4-PB (clone GK1.5), CXCR5-APC (clone L138D7), and CD19-A647 (clone 6D5), purchased from Biolegend; CD23-PE (clone B3B4), CD95-A647 (clone Jo2), CD44-FITC (clone IM7), and CD8-PE (clone 53-6.7), obtained from BD Biosciences; CD62L-APC (clone MEL-14), CD44-APC or -AlexaFluor700 (clone IM7), CD21-PECy7 (clone 8D9), GL7-A488 (clone GL7), CD3-PerCP-Cy5.5 or -PE-eFluor610 (clone 145-2C11), ICOSL-PE (clone HK5.3), B7.1-APC (clone 16-10A1), CD3-PE-eFluor610 (clone 17A2), CD8-APC, -SuperBright780 or -FITC (clone 53-6.7), CD4-FITC (clone GK1.5), CD45.1-SuperBright600 (clone A20), CD45.2-eFluor506 (clone 104), CD19-PE-eFluor610 (clone eBio1D3), NKp46-PE-eFluor610 (clone 29A1.4), CD11b-PE-Cy7 (clone M1/70), CD11c-PerCP-Cy5.5 (clone N418), MHC II-eFluor450 or –APC-eFluor780 (clone M5/114.15.2), TCR V alpha 11-APC (clone RR8-1 and IFN-γ (clone XMG1.2), from eBioscience, Thermo Fisher Scientific; PD-1-PE (clone J43.1) and CD3-PECy7 (clone 145-2C11), from Tonbo; and IgM-FITC (polyclonal), from Southern Biotech. Armenian hamster IgG (clone eBio299 Arm) and rat IgG2a kappa (clone eBR2a) isotype controls were purchased from Thermo Fisher Scientific. The rat anti-mouse ICOSL (clone HK5.3),

anti-mouse NK1.1 (clone PK136), anti-mouse CD8 (clone YTS 169.4), and anti-mouse CD4 (clone GK1.5) used for the *in vivo* assays were obtained from Bioxcell. The anti-mouse ICOSL (clone 599841) used for immunochemistry was purchased from Novusbio Biologicals. Biotin anti-human ICOSL (clone MIH12), CD4-APC (clone RPA-T4), and CD70 (clone 2F2) were purchased from ThermoFisher, BD Biosciences, and Immunotools, respectively. Anti-human ICOSL (polyclonal), anti-actin (clone C4), anti-HA (clone C2974), anti-GFP (polyclonal), and anti-human IE1 (clone 8B1.2), used for Western blots, were from Elabscience, MP Biomedicals, Cell Signaling MP, Abcam, and Merck Millipore, respectively. The anti-mouse IE1 (named Croma101) and the anti-human Fc IgG (clone 29.5; Fc specific) were previously described (Trgovcich et al., 2000; Pérez-Carmona N et al., 2015). Anti-mouse m04 (clones m04.17 or m04.16) antibody used as a marker of MCMV infection was produced in the Center for Proteomics (Faculty of Medicine, University of Rijeka, Croatia), and was described previously (Železnjak et al., 2019). The anti-mouse IgG-A555 was purchased from Life Technologies, the anti-rat IgG-A488 and anti-mouse IgG-PE or -A647 from Jackson ImmunoResearch, the anti-mouse IgG1-PerCP-eFluor710 and anti-mouse IgG2b-FITC from eBioscience, Thermo Fisher Scientific, the anti-rabbit IgG-HRP from Promega and the anti-mouse IgG-HRP from Sigma-Aldrich. The streptavidin-PE, -A555, or -HRP conjugates were purchased from BD Biosciences, ThermoFisher, and Roche, respectively. The anti-m138 mAb (clone m138.1.120) was generated by fusing an NS1 myeloma cell line with spleen cells from a BALB/c mouse immunized three times with 300.19 cells expressing at the cell surface HA-m138. The m138.1.120 mAb was subcloned and purified using an Affi-Gel protein A MAPS II kit (Bio-Rad) as indicated before (Engel et al., 2011). Fixable viability dye eFluor780 and eFluor506 (1000x, eBioscience, Thermo Fisher Scientific) were used to stain dead cells.

Plasmid constructions

HA-m138, containing the N-terminal HA-tagged m138 molecule without its signal peptide, was constructed by PCR using as a template DNA extracted from MCMV virions and primers m138PstIFor and m138PstIRev. The resulting PCR product was inserted into the pGEM-T vector, and subsequently, the *m138* fragment was excised with *Bgl*II and inserted in frame with the HA tag at the N-terminal end into the mammalian expression vector pDisplay (Invitrogen) opened with *Pst*I. The m138-GFP plasmid was obtained by PCR employing primers m138BamFor and m138BamRev, containing a *Bam*HI restriction site, and DNA from MCMV virions as a template. The PCR product was inserted into the pGEM-T vector, and then the m138 fragment without its terminal codon was excised with *Bam*HI and inserted in frame with the GFP at the C-terminal end into the pEGFP-N3 plasmid (clontech) opened with *Bam*HI. m138ΔIg1-GFP, without the first Ig domain of m138 (322nt-681nt), m138ΔIg2-GFP, without the second Ig domain of m138 (697nt-1029nt), and m138ΔIg2/3-GFP, without the second and third Ig domains of m138 (697nt-1416nt), were constructed as follows: first, independent PCR products were generated using as a template the pEGFP-N3 m138-GFP vector, two common external primers (m138BamFor and m138BamRev), and for each construct, two internal complementary primers bearing the corresponding deletions: SOEm138ΔIg1Rev and SOEm138ΔIg1For for m138ΔIg1; SOEm138ΔIg2Rev and SOEm138ΔIg2For for m138ΔIg2; and SOEm138ΔIg2/3Rev and SOEm138ΔIg2/3For for m138ΔIg2/3. Splicing by overhang extension (SOE)-PCR was then performed to join the two PCR fragments obtained for each m138 mutant using the external primers. These new PCR products were inserted into the pGEM-T vector, and then fragments of the m138 mutants without their terminal codon stop were excised and

cloned in frame with the GFP at the C-terminal end into the pEGFP-N3 plasmid opened with *Bam*HI. Mouse ICOSL, without its signal peptide, fused to the HA epitope at the N-terminus (HA-ICOSL) was obtained by PCR employing as a template pCMV6-mouse ICOSL vector (Origene) and primers ICOSLmurineSalIFor and ICOSLmurineNotIRev. The resulting PCR product was inserted into the pGEM-T vector and a *Sal*I-*Not*I fragment corresponding to the murine ICOSL was then excised and inserted into the mammalian expression vector pDisplay opened with the same restriction sites. In all cases, the PCR products inserted in the pGEM-T vector were sequenced to validate the nucleotide sequences, and when required, the correct orientations of the cloned inserts were assessed employing different restriction sites.

Flow cytometry analysis

Flow cytometry was performed according to the Guidelines for the use of flow cytometry and cell sorting in immunological studies (Cossarizza et al., 2017). To minimize non specific staining, all incubations were carried out in the presence of 20% rabbit serum (Linus) and 1% of fetal bovine serum in PBS. Adherent cells were harvested by incubation with 2 mM EDTA or when indicated by treatment with trypsin at 37ºC. For intracellular staining, cells were fixed and permeabilized with either the Intracellular fixation & permeabilization buffer set or Foxp3 staining buffer set (eBioscience) following manufacturer´s instructions, before antibody incubations. Prior to cytometry analysis cell suspensions from spleens, lungs, salivary glands and salivary gland draining lymph nodes were washed and filtered through a 70 μm cell strainer (Biologixs). All samples were acquired with LSRII Fortessa, FACSAria III or FACSCanto II flow cytometers (BD Biosciences) and analyzed with FlowJo Xv10.0.7

(Tree Star, Inc) software. At least two independent experiments were carried out for each subject of analysis.

Transient and stable transfections

NIH3T3 cells were transiently transfected with 2 μg of the corresponding plasmid using the Amaxa Cell Line Nucleofactor Kit R according to the manufacturer's protocol. Likewise, 300.19 and IC-21 cells were transfected employing the Amaxa Cell Line Nucleofector Kit V. To generate stable 300.19 cell lines expressing HA-m138 or NIH3T3 expressing HA-ICOSL, transfections were followed by G418 (Invitrogen) selection.

Western blot analysis

NIH3T3 and THP-1 cells were harvested by scrapping and extracts prepared in lysis buffer (20 mM Tris-HCl pH 7.5, 1 mM EDTA, 150 mM NaCl and 1% Triton X-100) supplemented with protease inhibitors (1 mM Na3VO4, 1 mM PMSF, 0.6 μg/mL Aprotinine, 2 μg/mL Leupeptin and 312 μg/mL Benzamidin). When specified, cells were previously incubated with 250 μM leupeptin and 20 nM bafilomycin A1 (Sigma). Lysates were quantified by a bicinchoninic acid (BCA) protein assay kit (ThermoScientific), and 15 μg of proteins were subjected to SDS-PAGE in 10% acrylamide gels and subsequently transferred to nitrocellulose membranes (Protran). The membranes were incubated with the indicated antibodies and blots were developed using the SuperSignal West Pico chemiluminescent substrate (Pierce) according to the manufacturer's protocol. Anti-actin mAb was used as a loading control, and anti-IE1 mAbs were used as infection controls. At least two independent experiments were carried out for each subject of analysis.

Immunoprecipitation

NIH3T3 cells non-trasfected or transfected with HA-ICOSL were surface labeled with biotin (Sigma-Aldrich) and lysed. Cell lysates were precleared 3 times for 30 min employing protein G-Sepharose (GE Healthcare) and immunoprecipitated by incubation with an anti-HA agarose conjugate (Sigma-Aldrich). Samples from immunoprecipitates were subjected to SDS-PAGE and Western blot analysis. Membranes were incubated with streptavidin-HRP or with anti-HA followed by anti-rabbit IgG-HRP. At least two independent experiments were carried out for each subject of analysis.

Co-Immunoprecipitation

NIH3T3 cells co-transfected with m138-GFP and HA-ICOSL were lysed with a soft lysis buffer (20 mM Tris HCl pH 8, 100mM NaCl, 2mM EDTA and 0.5% Triton-X-100) supplemented with Halt protease inhibitor cocktail, during 30 minutes at 4ºC. The lysates were incubated with G-Sepharose beads in three rounds for 30 minutes each, followed by an overnight incubation with an anti-HA agarose conjugate. The immunoprecipitates were washed four times with Co-IP lysis buffer before the samples were subjected to Western blot analysis. Membranes were incubated with anti-GFP or with anti-HA, followed by an anti-rabbit IgG-HRP. At least two independent experiments were carried out for each subject of analysis.

Immunofluorescence microscopy

NIH3T3 cells and 300.19 cells, either untransfected or stably transfected with HA-ICOSL or HA-m138, respectively, were cultured on glass coverslips in 24-well tissue

culture plates. When specified, NIH3T3 cells were MCMV infected and exposed to lysosomal inhibitors as indicated for the Western blot analysis. At 24 hpi, cells were washed in PBS and fixed and permeabilized using 4% paraformaldehyde and 0.05% Triton X-100 (for intracellular staining), or just fixed in paraformaldehyde (for cell surface detection), and subsequently blocked with PBS 6% FBS. Cells were stained with anti-m138 mAb or anti-ICOSL, using as secondary antibodies an anti-mouse IgG-A555 or an anti-rat IgG-A488. Nuclei were counterstained with DAPI reagent (Invitrogen). In assays where the LysoTracker Red DND-99 (Molecular Probes) was used, cells were incubated at 37°C for 2 hours with 100 nM of the fluorescence dye, fixed with 4% paraformaldehyde, gently permeabilized with 0.02% saponin, and immediately processed as indicated above. In this case, the anti-m138 mAb and an anti-mouse IgG-A488 were used. The samples were mounted in ProLong Gold antifade reagent (Invitrogen). Cells were examined under a fluorescence microscope at 405 nm (DAPI), at 555-565 nm (A555), and at 495-518 (A488). GFP was observed at 450-490. Fluorescence images were obtained using a Nikon Eclipse E600 microscope (Nikon) or an inverted Leica DMI6000B microscope and the LAS AF software from Leica Microsystems (Leica, Wetzlar). A Zeiss LSM880 laser scanning spectral confocal microscope (Zeiss, Jena) equipped with an Axio Observer 7 inverted microscope, blue diode (405nm), Argon (488nm), diode pumped solid state (561nm) and HeNe (633nm) lasers and a Plan Apochromat 63x oil (NA 1.4) immersion objective lenses was also used. DAPI, A-488 and A-555 images were acquired sequentially using 405, 488 and 561 laser lines, AOBS (Acoustic Optical Beam Splitter) as beam splitter and emission detection ranges 415- 480, 500-550 nm, and 571-625nm, respectively, and the confocal pinhole set at 1 Airy units. Spectral detection was performed using 2 photomultipliers and one central GaAsP detector. Analysis of the co-localization of m138 and the

LysoTracker red fluorescence was determined using the ImageJ software analyzing 20 cells from each sample. Colocalization was assessed using Coloc2 plugin from FIJI/ImageJ program (Schindelin et al., 2019). A macro of instructions was created to process and automate colocalization quantification. Briefly, red and green channel images were background substracted with Rolling Ball Radius of 50 and colocalization was quantified from a region of interest delimiting the cell contour. Manders coefficients were analyzed from each image. M2 Manders colocalization coefficient indicates the percentage of m138 colocalizing with lysosomes, and M1 Manders cocoefficient the percentage of lysosomes colocalizing with m138. At least two independent experiments were carried out for each subject of analysis.

Immunohistochemistry

Mice were euthanized at the indicated time points and spleens immediately collected within O.C.T. (Sakura) cryo-embedding media at -80°C. Consecutive tissue sections of 2.5 µm were obtained in the cryostat and fixed/permeabilized in acetone. Unspecific binding was prevented with PBS 6% FBS blocking solution. Antigens were detected with a rat anti-mouse CD45R/B220 and PNA (peanut lectin) biotin (Sigma-Aldrich). After 1 hour of incubation at room temperature, B220 antigen was revealed with anti-rat IgG- A488 and PNA with streptavidin-A555. Labeled tissue sections were visualized with a fluorescence microscope. Four consecutive tissue sections were evaluated from three representative mice of each experimental group. Follicle and germinal center areas were calculated from the total spleen sections of one representative mice of each group using ImageJ software. At least two independent experiments were carried out for each subject of analysis.

Mouse infections, antibody treatment and determination of viral titers

Four-week-old BALB/c mice (females and males) were obtained from Harlan (Netherlands) and housed in the vivarium of the Medical School of the University of Barcelona under specific-pathogen-free (SPF) conditions. Eight-to-twelve-week-old C57BL/6, TCR transgenic mice specific for M38 (Maxi mice; Torti et al., 2011), TCR transgenic mice specific for M25-II (Mandaric et al., 2012), C57BL/6 SCID and BALB/c mice were housed and bred under SPF conditions at the Central Animal Facility of the Medical Faculty of the University of Rijeka. When specified, ICOSL was blocked by i.p. injection of a rat anti-mouse ICOSL monoclonal antibody (clone HK5.3) at a concentration of 100 µg per mouse. The monoclonal antibody was administrated one day before infection and on days 2, 5, 8 and 11 after infection. The efficacy of the *in vivo* ICOSL blockade was assessed by cytofluorometric analyses of spleen cells from treated mice using an anti-ICOSL recognizing the same epitope than the antibody used in the *in vivo* assay. For these assays, mice were i.p. inoculated with $2.5x10^6$ PFU/mouse of tissue culture-propagated MCMVΔm138. Mice were observed and weighed during all the experiment and at 14 days post infection, animals were sacrificed, and specific organs were removed, and their sera collected. Salivary gland and lungs were harvested as a 10% (weight/volume) tissue homogenate. Tissue homogenates were sonicated and centrifuged, and viral titers from the supernatants of individual mice were determined by standard plaque assays in MEFs, including a centrifugal enhancement of infectivity step. In experiments evaluating the *in vivo* effect of MCMV infection on ICOSL surface levels, mice were i.p. inoculated with $2x10^6$ PFU/mouse of MCMV-GFP, and 2 days after infection, cells present in the peritoneal cavity were harvested with 5 mL of PBS and analyzed by flow cytometry. In depleting assays, eight-to-twelve-week-old C57BL/6 mice were infected i.v. with $2x10^5$

PFU/mouse of MCMVwt, MCMVΔm138, or MCMVm138ΔIg2. On the day of infection and on days 5^{th} and 10^{th} after infection, indicated groups of mice were injected i.p. with 250 µg of anti-mouse NK1.1, 150 µg of anti-CD8, or 150 µg anti-mouse CD4 depleting antibodies. At day 14 post infection, mice were sacrificed and viral titers in salivary glands and lungs of individual mice were determined by standard plaque assays. To obtain high-dose systemic infection, BALB/c mice were inoculated i.p. with 10^6 PFU/mouse of MCMVwt or MCMVΔm138 for 6 hours after which peritoneal exudate cells were isolated according to Ray and Dittel (2010). At least two independent experiments were carried out for each subject of analysis.

Adoptive transfer assay

C57BL/6 SCID mice were i.p. infected with $2x10^5$ PFU/mouse of MCMVwt or MCMVΔm138. One day prior to infection, mice were first injected i.p. with 250 µg of anti-mouse NK1.1 and a few hours later were given 10^5 M25-II $CD4^+$ T cells. Another NK cell depletion followed on day 3 post infection. Spleen, lungs and salivary glands were isolated 7 days after infection and the expansion of $CD4^+$ T cell ($CD45.1^+$ $CD4^+$) was analyzed. M25-II $CD4^+$ T cells were obtained from naive C57BL/6 transgenic M25-II mice. Briefly, splenocytes from C57BL/6 M25-II mice were isolated and enriched using $CD4^+$ T Cell Isolation Kit (Miltenyi). Percentage of M25-II $CD4^+$ T cells was obtained by staining with TCR V alpha 11 (clone RR8-1, eBioscience ThermoFisher) antibody.

***In vitro* stimulation of $CD8^+$ T cells**

C57BL/6 BMDCs were infected with 3 PFU/cell of indicated viruses. After 24 hours of infection, splenocytes from naive Maxi mice were added at the different T:E

(BMDCs:$CD8^+$) ratios to infected BMDCs together with Brefeldin A (eBioscience, Thermo Fisher Scientific). After 6 hours of co-cultivation, IFN-γ production by $CD8^+$ T cells was measured. At least three independent experiments were carried out for each subject of analysis with two technical replicates/experiment.

Quantification of serum anti-MCMV antibody levels

Detection of antibodies against MCMV on sera of MCMV-infected mice was performed by sandwich ELISA using 1.5 μg/well of MCMVΔm138-infected MEF lysate to coat the ELISA plates as described in Miletic et al., 2017. Briefly, $5x10^6$ MEFs were infected with 0.01 PFU/cell with MCMVΔm138 until a high infection was reached after 5 days. Cells were then harvested by incubation with 2 mM EDTA and washed twice with cold PBS. Cells were sonicated in bicarbonate buffer, quantified by BCA and stored at -20ºC. Diluted sera were incubated for 2 hours on the coated plates, followed by incubation with anti-mouse IgG-HRP to measure total IgGs, or with anti-mouse IgG1, IgG2a, IgG2b, IgG3 or IgM biotin conjugated (Jackson ImmunoResearch), followed by streptavidin-HRP. After washing, freshly prepared TMB substrate solution was added and the absorbance was measured at 450 and 570 nm wavelength (Thermo Scientific Multiskan FC). At least two independent experiments were carried out for each subject of analysis with at least two technical replicates/experiment.

***In vitro* neutralization**

Collected sera from MCMV infected mice were decomplemented at 56°C for 30 minutes, and then incubated, at the indicated dilution, with 100 PFU of the MCMV-GFP in DMEM containing or not 25% of rabbit serum for 1 hour at 37°C. The mixtures were then transferred to monolayers of MEFs p53 grown in wells of 24-well plates, and

1043 further incubated 1 hour at 37°C. Next, cells were covered with medium containing
1044 0.25% agarose and lysis plaques produced after 5-7 days in each condition counted.
1045 Results were represented as the percentage of plaque reduction, determined by the ratio
1046 of the amount of the plaques counted in the sample wells relative to the amount of
1047 plaques visualized in wells containing the serum of an uninfected mouse. At least two
1048 independent experiments were carried out for each subject of analysis with at least three
1049 technical replicates/experiment.
1050
1051 **Statistical analyses**
1052 Results are expressed as mean +/- standard deviation (SD) or standard error of the mean
1053 (SEM) of at least three independent experiments. For *in vivo* experiments, mice were
1054 pooled and randomized in experimental groups from 4 to 6 animals. The sample size
1055 was determined by pilot studies and according to the accepted practices in previous
1056 literature using the MCMV model. The selection of the appropriate statistical test was
1057 based on the number and distribution of data points per set. Differences between group
1058 means or individual values were assessed using the unpaired two-tailed *t*-test. Statistical
1059 differences between more than two study groups were evaluated using either the one-
1060 way ANOVA test or the Kruskal-Wallis bidirectional test. Exact *p*-values considered
1061 statistically significant and statistical details of experiments are indicated in the figure
1062 legends. All statistical analyses were performed using GraphPad Prism software version
1063 7.03 and 8.1.1.
1064
1065 The key Resources Table (Supplementary File 1) lists the key reagents used in this
1066 study.

Acknowledgements

We thank Adriana Lázaro for technical assistance with the production of the monoclonal antibody against m138, Manuel Eduardo Sáez Moya for help in the preparation of histological tissue sections, and Francesc Poblador and Pablo Hernández-Luis for technical assistance in the immunohistochemistry assays. We acknowledge the use of the Advanced Optical Microscopy Facility at the University of Barcelona, and María Calvo for the analysis of confocal fluorescence microscopy images. We also thank Antonio Alcamí (Autonomous University of Madrid, Spain) for providing HSV-1 and HSV-2 expressing GFP. In addition, we would like to thank Lea Hiršl, Tina Jenuš and Maja Cokarić Brdovčak for the help involving adoptive transfer assay and genotyping of C57BL/6 M25-II mice.

Competing interests

No competing interests declared.

Funding

The study was supported by the Ministerio de Economia y Competitividad (MINECO, Spain) through grants SAF 2017-87688 (to Angulo A.), and RTI2018-094440-B-I00 (to Engel P.), by the grant "Strengthening the capacity of CerVirVac for research in virus immunology and vaccinology", KK.01.1.1.01.0006, awarded to the Scientific Centre of Excellence for Virus Immunology and Vaccines and co-financed by the European Regional Development Fund (to Jonjic S.), by the University of Rijeka under the project number uniri-biomed-18-170 (to Krmpotić A.), by the Croatian-Swiss Research Program of the Croatian Science Foundation and the Swiss National Science Foundation with funds obtained from the Swiss-Croatian Cooperation Programme (to

1092 Oxenius A. and Krmpotić A.), and by the Deutsche Forschungsgemeinschaft (DFG,
1093 German Research Foundation) – Projektnummer 421451057 – FOR2830 (to Messerle
1094 M. and Jonjic S.) and HE2526/9-1 (to Hengel H.). Angulo G., and Puñet-Ortiz J. were
1095 supported by a Formación de Personal Investigador fellowship (MINECO).

References

Aicher A, Hayden-Ledbetter M, Brady WA, Pezzutto A, Richter G, Magaletti D, Buckwalter S, Ledbetter JA, Clark EA. Characterization of human inducible costimulator ligand expression and function. J Immunol. 2000;164(9):4689-96. DOI: 10.4049/jimmunol.164.9.4689

Arapović J, Lenac Rovis T, Reddy AB, Krmpotić A, Jonjić S. Promiscuity of MCMV immunoevasin of NKG2D: m138/fcr-1 down-modulates RAE-1epsilon in addition to MULT-1 and H60. Mol Immunol. 2009;47(1):114-22. DOI: 10.1016/j.molimm.2009.02.010

Arens R, Loewendorf A, Her MJ, Schneider-Ohrum K, Shellam GR, Janssen E, Ware CF, Schoenberger SP, Benedict CA. B7-mediated costimulation of CD4 T cells constrains cytomegalovirus persistence. J Virol. 2011;85(1):390-6. DOI:10.1128/JVI.01839-10

Bertram EM, Tafuri A, Shahinian A, Chan VS, Hunziker L, Recher M, Ohashi PS, Mak TW, Watts TH. Role of ICOS versus CD28 in antiviral immunity. Eur J Immunol. 2002;32(12):3376-85.DOI:10.1002/1521-4141(200212)32:12<3376::AID-IMMU3376>3.0.CO;2-Y

Brinkmann MM, Dağ F, Hengel H, Messerle M, Kalinke U, Čičin-Šain L. Cytomegalovirus immune evasion of myeloid lineage cells. Med Microbiol Immunol. 2015;204(3):367-82. DOI:10.1007/s00430-015-0403-4

1121

1122 Brune W, Wagner M, Messerle M. Manipulating cytomegalovirus genomes by BAC
1123 mutagenesis: Strategies and applications, *in* Reddehase, M.J. *(ed.)* Cytomegaloviruses,
1124 Molecular Biology and Immunology. (Vol. 1). Caister Academic Press. Norfolk, UK.
1125 2006;63-89.

1126

1127 Budt M, Reinhard H, Bigl A, Hengel H. Herpesviral Fcgamma receptors: culprits
1128 attenuating antiviral IgG? Int Immunopharmacol. 2004;4(9):1135-48.
1129 DOI:10.1016/j.intimp.2004.05.020

1130

1131 Cavanaugh VJ, Stenberg RM, Staley TL, Virgin HW 4th, MacDonald MR, Paetzold S,
1132 Farrell HE, Rawlinson WD, Campbell AE. Murine cytomegalovirus with a deletion of
1133 genes spanning HindIII-J and -I displays altered cell and tissue tropism. J Virol.
1134 1996;70(3):1365-74.

1135

1136 Chen L, Flies DB. Molecular mechanisms of T cell co-stimulation and co-inhibition.
1137 Nat Rev Immunol. 2013;13(4):227-42. DOI:10.1038/nri3405

1138

1139 Choi YS, Kageyama R, Eto D, Escobar TC, Johnston RJ, Monticelli L, Lao C, Crotty S.
1140 ICOS receptor instructs T follicular helper cell versus effector cell differentiation via
1141 induction of the transcriptional repressor Bcl6. Immunity. 2011;34(6):932-46.
1142 DOI:10.1016/j.immuni.2011.03.023

1143

1144 Clement M, Marsden M, Stacey MA, Abdul-Karim J, Gimeno Brias S, Costa Bento D,
1145 Scurr MJ, Ghazal P, Weaver CT, Carlesso G, Clare S, Jones SA, Godkin A, Jones GW,

1146 Humphreys IR. Cytomegalovirus-specific IL-10-Producing CD4+ T Cells are governed
1147 by type-I IFN-induced IL-27 and promote virus persistence. PLoS Pathog.
1148 2016;12(12):e1006050. DOI: 10.1371/journal.ppat.1006050
1149
1150 Corrales-Aguilar E, Hoffmann K, Hengel H. CMV-encoded Fcγ receptors: modulators
1151 at the interface of innate and adaptive immunity. Semin Immunopathol.
1152 2014;36(6):627-40.
1153 DOI:10.1007/s00281-014-0448-2
1154
1155 Cossarizza A, Chang HD, Radbruch A, Acs A, Adam D, Adam-Klages S, et al.
1156 Guidelines for the use of flow cytometry and cell sorting in immunological studies
1157 (second edition). Eur J Immunol. 2019;49(10):1457-973. DOI:10.1002/eji.201970107
1158
1159 Coyle AJ, Lehar S, Lloyd C, Tian J, Delaney T, Manning S, Nguyen T, Burwell T,
1160 Schneider H, Gonzalo JA, Gosselin M, Owen LR, Rudd CE, Gutierrez-Ramos JC. The
1161 CD28-related molecule ICOS is required for effective T cell-dependent immune
1162 responses. Immunity. 2000;13(1):95-105. DOI:10.1016/s1074-7613(00)00011-x
1163
1164 Crnković-Mertens I, Messerle M, Milotić I, Szepan U, Kucić N, Krmpotić A, Jonjić S,
1165 Koszinowski UH. Virus attenuation after deletion of the cytomegalovirus Fc receptor
1166 gene is not due to antibody control. J Virol. 1998;72(2):1377-82.
1167
1168 Engel P, Pérez-Carmona N, Albà MM, Robertson K, Ghazal P, Angulo A. Human
1169 cytomegalovirus UL7, a homologue of the SLAM-family receptor CD229, impairs
1170 cytokine production. Immunol Cell Biol. 2011;89(7):753-66. DOI:10.1038/icb.2011.55

Fielding CA, Weekes MP, Nobre LV, Ruckova E, Wilkie GS, Paulo JA, Chang C, Suárez NM, Davies JA, Antrobus R, Stanton RJ, Aicheler RJ, Nichols H, Vojtesek B, Trowsdale J, Davison AJ, Gygi SP, Tomasec P, Lehner PJ, Wilkinson GW. Control of immune ligands by members of a cytomegalovirus gene expansion suppresses natural killer cell activation. Elife. 2017;6. pii: e22206. DOI:10.7554/eLife.22206

Fink A, Renzaho A, Reddehase MJ, Lemmermann NA. The p36 isoform of murine cytomegalovirus m152 protein suffices for mediating innate and adaptive immune evasion. Viruses. 2013;5(12):3171-91. DOI: 10.3390/v5123171

Fleming P, Davis-Poynter N, Degli-Esposti M, Densley E, Papadimitriou J, Shellam G, Farrell H. The murine cytomegalovirus chemokine homolog, m131/129, is a determinant of viral pathogenicity. J Virol. 1999;73(8):6800-9. DOI: 10.1128/JVI.73.8.6800-6809.1999

Gewurz BE, Vyas JM, Ploegh HL. Herpesvirus evasion of T-cell immunity. In: Arvin A, Campadelli-Fiume G, Mocarski E, Moore PS, Roizman B, Whitley R, Yamanishi K, editors. Human Herpesviruses: Biology, Therapy, and Immunoprophylaxis. Cambridge: Cambridge University Press. 2007. Chapter 62. PubMed PMID: 21348103.

Hertel L, Lacaille VG, Strobl H, Mellins ED, Mocarski ES. Susceptibility of immature and mature Langerhans cell-type dendritic cells to infection and immunomodulation by human cytomegalovirus. J Virol. 2003;77(13):7563-74. DOI:10.1128/jvi.77.13.7563-7574.2003

Hudson JB. Further studies on the mechanism of centrifugal enhancement of cytomegalovirus infectivity. J Virol Methods. 1988;19(2):97-108. DOI:10.1016/0166-0934(88)90153-x

Hutloff A, Dittrich AM, Beier KC, Eljaschewitsch B, Kraft R, Anagnostopoulos I, Kroczek RA. ICOS is an inducible T-cell co-stimulator structurally and functionally related to CD28. Nature. 1999;397(6716):263-6. DOI:10.1038/16717

Hutloff A. Regulation of T follicular helper cells by ICOS. Oncotarget. 2015;6(26):21785-6. DOI: 10.18632/oncotarget.4798

Khan N, Gowthaman U, Pahari S, Agrewala JN. Manipulation of costimulatory molecules by intracellular pathogens: veni, vidi, vici!! PLoS Pathog. 2012;8(6):e1002676. DOI:10.1371/journal.ppat.1002676

Khayyamian S, Hutloff A, Büchner K, Gräfe M, Henn V, Kroczek RA, Mages HW. ICOS-ligand, expressed on human endothelial cells, costimulates Th1 and Th2 cytokine secretion by memory CD4+ T cells. Proc Natl Acad Sci U S A. 2002;99(9):6198-203. DOI:10.1073/pnas.092576699

Kopf M, Coyle AJ, Schmitz N, Barner M, Oxenius A, Gallimore A, Gutierrez-Ramos JC, Bachmann MF. Inducible costimulator protein (ICOS) controls T helper cell subset polarization after virus and parasite infection. J Exp Med. 2000;192(1):53-61. DOI:10.1084/jem.192.1.53

Krmpotić A, Messerle M, Crnkovic-Mertens I, Polic B, Jonjic S, Koszinowski UH. The immunoevasive function encoded by the mouse cytomegalovirus gene m152 protects the virus against T cell control in vivo. J Exp Med. 1999;190(9):1285-96. DOI: 10.1084/jem.190.9.1285

Lenac T, Budt M, Arapović J, Hasan M, Zimmermann A, Simic H, Krmpotic A, Messerle M, Ruzsics Z, Koszinowski UH, Hengel H, Jonjic S. The herpesviral Fc receptor fcr-1 down-regulates the NKG2D ligands MULT-1 and H60. J Exp Med. 2006;203(8):1843-50. DOI:10.1084/jem.20060514

Liu D, Xu H, Shih C, Wan Z, Ma X, Ma W, Luo D, Qi H. T-B-cell entanglement and ICOSL-driven feed-forward regulation of germinal centre reaction. Nature. 2015;517(7533):214-8. DOI:10.1038/nature13803

Lodoen M, Ogasawara K, Hamerman JA, Arase H, Houchins JP, Mocarski ES, Lanier LL. NKG2D-mediated natural killer cell protection against cytomegalovirus is impaired by viral gp40 modulation of retinoic acid early inducible 1 gene molecules. J Exp Med. 2003;197(10):1245-53. DOI:10.1084/jem.20021973

Loewendorf A, Krüger C, Borst EM, Wagner M, Just U, Messerle M. Identification of a mouse cytomegalovirus gene selectively targeting CD86 expression on antigen-presenting cells. J Virol. 2004;78(23):13062-71. DOI: 10.1128/JVI.78.23.13062-13071.2004

Mandaric S, Walton SM, Rülicke T, Richter K, Girard-Madoux MJ, Clausen BE, Zurunic A, Kamanaka M, Flavell RA, Jonjic S, Oxenius A. IL-10 suppression of NK/DC crosstalk leads to poor priming of MCMV-specific CD4 T cells and prolonged MCMV persistence. PLoS Pathog. 2012;8(8):e1002846. DOI: 10.1371/journal.ppat.1002846

Mathys S, Schroeder T, Ellwart J, Koszinowski UH, Messerle M, Just U. Dendritic cells under influence of mouse cytomegalovirus have a physiologic dual role: to initiate and to restrict T cell activation. J Infect Dis. 2003;187(6):988-99. DOI:10.1086/368094

Miletic A, Lenartic M, Popovic B, Brizic I, Trsan T, Miklic K, Mandelboim O, Krmpotic A, Jonjic S. NCR1-deficiency diminishes the generation of protective murine cytomegalovirus antibodies by limiting follicular helper T-cell maturation. Eur J Immunol. 2017;47(9):1443-56. DOI:10.1002/eji.201646763

Mintern JD, Klemm EJ, Wagner M, Paquet ME, Napier MD, Kim YM, Koszinowski UH, Ploegh HL. Viral interference with B7-1 costimulation: a new role for murine cytomegalovirus fc receptor-1. J Immunol. 2006;177(12):8422-31. DOI:10.4049/jimmunol.177.12.8422

Moutaftsi M, Mehl AM, Borysiewicz LK, Tabi Z. Human cytomegalovirus inhibits maturation and impairs function of monocyte-derived dendritic cells. Blood. 2002;99(8):2913-21. DOI:10.1182/blood.v99.8.2913

Ogasawara K, Yoshinaga SK, Lanier LL. Inducible costimulator costimulates cytotoxic activity and IFN-gamma production in activated murine NK cells. J Immunol. 2002;169(7):3676-85. DOI:10.4049/jimmunol.169.7.3676

Pérez-Carmona N, Farré D, Martínez-Vicente P, Terhorst C, Engel P, Angulo A. Signaling lymphocytic activation molecule family receptor homologs in new world monkey cytomegaloviruses. J Virol. 2015;89:11323-36. DOI:10.1128/JVI.01296-15

Qian X, Agematsu K, Freeman GJ, Tagawa Y, Sugane K, Hayashi T. The ICOS-ligand B7-H2, expressed on human type II alveolar epithelial cells, plays a role in the pulmonary host defense system. Eur J Immunol. 2006;36(4):906-18. DOI:10.1002/eji.200535253

Ray A, Dittel BN. Isolation of mouse peritoneal cavity cells. J Vis Exp. 2010;(35):1488. DOI:10.3791/1488

Riley JL, Mao M, Kobayashi S, Biery M, Burchard J, Cavet G, Gregson BP, June CH, Linsley PS. Modulation of TCR-induced transcriptional profiles by ligation of CD28, ICOS, and CTLA-4 receptors. Proc Natl Acad Sci U S A. 2002;99(18):11790-5. DOI:10.1073/pnas.162359999

Roussel L, Landekic M, Golizeh M, Gavino C, Zhong MC, Chen J, Faubert D, Blanchet-Cohen A, Dansereau L, Parent MA, Marin S, Luo J, Le C, Ford BR, Langelier M, King IL, Divangahi M, Foulkes WD, Veillette A, Vinh DC. Loss of human ICOSL results in combined immunodeficiency. J Exp Med. 2018;215(12):3151-64.

DOI:10.1084/jem.20180668

Schepp J, Chou J, Skrabl-Baumgartner A, Arkwright PD, Engelhardt KR, Hambleton S, Morio T, Röther E, Warnatz K, Geha R, Grimbacher B. 14 Years after discovery: clinical follow-up on 15 patients with inducible co-stimulator deficiency. Front Immunol. 2017;8:964. DOI:10.3389/fimmu.2017.00964

Schindelin J, Arganda-Carreras I, Frise E, Kaynig V, Longair M, Pietzsch T, Preibisch S, Rueden C, Saalfeld S, Schmid B, Tinevez JY, White DJ, Hartenstein V, Eliceiri K, Tomancak P, Cardona A. Fiji: an open-source platform for biological-image analysis. Nat Methods. 2012 28;9(7):676-82. DOI: 10.1038/nmeth.2019

Schuren AB, Costa AI, Wiertz EJ. Recent advances in viral evasion of the MHC Class I processing pathway. Curr Opin Immunol. 2016;40:43-50. DOI:10.1016/j.coi.2016.02.007

Sharpe AH, Freeman GJ. The B7-CD28 superfamily. Nat Rev Immunol. 2002;2(2):116-26. DOI:10.1038/nri727

Sharpe AH. Mechanisms of costimulation. Immunol Rev. 2009;229(1):5-11. DOI: 10.1111/j.1600-065X.2009.00784.x

Sinzger C, Hahn G, Digel M, Katona R, Sampaio KL, Messerle M, Hengel H, Koszinowski U, Brune W, Adler B. Cloning and sequencing of a highly productive,

endotheliotropic virus strain derived from human cytomegalovirus TB40/E. J Gen Virol. 2008;89(Pt 2):359-68. DOI:10.1099/vir.0.83286-0

Stahl FR, Keyser KA, Heller K, Bischoff Y, Halle S, Wagner K, Messerle M, Förster R. Mck2-dependent infection of alveolar macrophages promotes replication of MCMV in nodular inflammatory foci of the neonatal lung. Mucosal Immunol. 2015;8(1):57-67. DOI:10.1038/mi.2014.42

Stempel M, Chan B, Juranić Lisnić V, Krmpotić A, Hartung J, Paludan SR, Füllbrunn N, Lemmermann NA, Brinkmann MM. The herpesviral antagonist m152 reveals differential activation of STING-dependent IRF and NF-κB signaling and STING's dual role during MCMV infection. EMBO J. 2019;38(5). pii: e100983. DOI:10.15252/embj.2018100983

Strazic Geljic I, Kucan Brlic P, Angulo G, Brizic I, Lisnic B, Jenus T, Juranic Lisnic V, Pietri GP, Engel P, Kaynan N, Zeleznjak J, Schu P, Mandelboim O, Krmpotic A, Angulo A, Jonjic S, Lenac Rovis T. Cytomegalovirus protein m154 perturbs the adaptor protein-1 compartment mediating broad-spectrum immune evasion. Elife. 2020;9. pii: e50803. DOI:10.7554/eLife.50803

Swallow MM, Wallin JJ, Sha WC. B7h, a novel costimulatory homolog of B7.1 and B7.2, is induced by TNFalpha. Immunity. 1999;11(4):423-32. DOI:10.1016/s1074-7613(00)80117-x

Takahashi N, Matsumoto K, Saito H, Nanki T, Miyasaka N, Kobata T, Azuma M, Lee SK, Mizutani S, Morio T. Impaired CD4 and CD8 effector function and decreased memory T cell populations in ICOS-deficient patients. J Immunol. 2009;182(9):5515-27.
DOI:10.4049/jimmunol.0803256

Tesciuba AG, Subudhi S, Rother RP, Faas SJ, Frantz AM, Elliot D, Weinstock J, Matis LA, Bluestone JA, Sperling AI. Inducible costimulator regulates Th2-mediated inflammation, but not Th2 differentiation, in a model of allergic airway disease. J Immunol. 2001;167(4):1996-2003. DOI:10.4049/jimmunol.167.4.1996

Thäle R, Lucin P, Schneider K, Eggers M, Koszinowski UH. Identification and expression of a murine cytomegalovirus early gene coding for an Fc receptor. J Virol. 1994;68(12):7757-65.

Torti N, Walton SM, Brocker T, Rülicke T, Oxenius A. 2011. Non-hematopoietic cells in lymph nodes drive memory CD8 T cell inflation during murine cytomegalovirus infection. PLoS Pathog. 2011;7:e1002313. DOI: 10.1371/journal.ppat.1002313

Trgovcich J, Stimac D, Polić B, Krmpotić A, Pernjak-Pugel E, Tomac J, Hasan M, Wraber B, Jonjić S. Immune responses and cytokine induction in the development of severe hepatitis during acute infections with murine cytomegalovirus. Arch Virol. 2000;145(12):2601-18. DOI:10.1007/s007050070010

Wagner M, Jonjic S, Koszinowski UH, Messerle M. Systematic excision of vector sequences from the BAC-cloned herpesvirus genome during virus reconstitution. J Virol. 1999;73(8):7056-60.

Wallin JJ, Liang L, Bakardjiev A, Sha WC. Enhancement of CD8+ T cell responses by ICOS/B7h costimulation. J Immunol. 2001;167(1):132-9. DOI:10.4049/jimmunol.167.1.132

Welten SPM, Redeker A, Toes REM, Arens R. Viral persistence induces antibody inflation without altering antibody avidity. J Virol. 2016;90(9):4402-11. DOI:10.1128/JVI.03177-15

Wikenheiser DJ, Stumhofer JS. ICOS Co-Stimulation: Friend or Foe? Front Immunol. 2016;7:304. DOI:10.3389/fimmu.2016.00304

Yoshinaga SK, Whoriskey JS, Khare SD, Sarmiento U, Guo J, Horan T, Shih G, Zhang M, Coccia MA, Kohno T, Tafuri-Bladt A, Brankow D, Campbell P, Chang D, Chiu L, Dai T, Duncan G, Elliott GS, Hui A, McCabe SM, Scully S, Shahinian A, Shaklee CL, Van G, Mak TW, Senaldi G. T-cell co-stimulation through B7RP-1 and ICOS. Nature. 1999;402(6763):827-32. DOI:10.1038/45582

Yoshinaga SK, Zhang M, Pistillo J, Horan T, Khare SD, Miner K, Sonnenberg M, Boone T, Brankow D, Dai T, Delaney J, Han H, Hui A, Kohno T, Manoukian R, Whoriskey JS, Coccia MA. Characterization of a new human B7-related protein: B7RP-

1 is the ligand to the co-stimulatory protein ICOS. Int Immunol. 2000;12(10):1439-47. DOI:10.1093/intimm/12.10.1439

Zarama A, Pérez-Carmona N, Farré D, Tomic A, Borst EM, Messerle M, Jonjic S, Engel P, Angulo A. Cytomegalovirus m154 hinders CD48 cell-surface expression and promotes viral escape from host natural killer cell control. PLoS Pathog. 2014;10(3):e1004000. DOI:10.1371/journal.ppat.1004000

Železnjak J, Lisnić VJ, Popović B, Lisnic B, Babic M, Halenius A, L'Hernault A, Lenac Rovis A, Hengel H, Erhard F, Redwood AJ, Vidal SM, Dölken L, Krmpotić A, Jonjic S. The complex of MCMV proteins and MHC class I evades NK cell control and drives the evolution of virus-specific activating Ly49 receptors. J Exp Med. 2019;216(8):1809-27. DOI: 10.1084/jem.20182213

Ziegler H, Thale R, Lucin P, Muranyi W, Flohr T, Hengel H, Farrell H, Rawlinson W, Koszinowski UH. A mouse cytomegalovirus glycoprotein retains MHC class I complexes in the ERGIC/cis-Golgi compartments. Immunity. 1997;6(1):57-66. DOI: 10.1016/s1074-7613(00)80242-3

Figure legends

Figure 1. Downregulation of ICOSL upon MCMV infection of APCs. (A) Peritoneal macrophages (MΦ) were mock-infected or infected for 72 hours with MCMV-GFP at an moi of 5 and analyzed by flow cytometry for surface expression of ICOSL, MHC I, or CD62L using specific mAbs against each of these molecules. Grey histograms represent the expression on mock-infected cells, green histograms represent the expression on MCMV-infected (GFP+) cells, and blue histograms represent the expression on uninfected (GFP-) cells from the same culture. (B) Bone marrow derived-macrophages (BMM), bone marrow derived-dendritic cells (BMDC), IC-21, DC2.4, and SVEC4-10 cells were infected with MCMV-GFP at different moi (10, 20, 20, and 5, respectively) to obtain an infection of around 50% of the cell culture, and analyzed by flow cytometry for surface expression of ICOSL. Grey, green, and blue histograms, as indicated in A. (C) Same as in A, except that peritoneal macrophages were infected with MCMV-GFP at an moi of 10, or treated for 72 h with the same amount of MCMV-GFP UV-inactivated. Grey and green as indicated in A, and red histograms represent the expression on MCMV-GFP UV-inactivated infected cells. (D) Peritoneal macrophages, BMDCs, and IC-21 cells were mock-infected (time 0) or infected with MCMV-GFP at an moi of 10, 40 and 20, respectively, and analyzed by flow cytometry for surface expression of ICOSL at the different time points after infection indicated. In A, B, C, and D, the isotype for each antibody was used as a negative control (dotted lines). Data are representative of at least two independent experiments.

Figure 2. Identification of the MCMV gene involved in the decreased cell surface expression of ICOSL. (A) IC-21 cells were mock-infected or infected for 72 h with

MCMV-GFP, MCMV-GFPΔm128-m138, or MCMV-GFPΔm1-m17 at an moi of 10 and examined by flow cytometry for surface expression of ICOSL. Grey histograms represent the expression of mock-infected cells, green histograms represent the expression on MCMV-infected (GFP+) cells, and blue histograms represent the expression on uninfected (GFP-) cells from the same culture. (B) IC-21 cells were mock-infected or infected with MCMVwt or MCMVΔm138 for 72h at an moi of 20 and analyzed by flow cytometry for surface expression of ICOSL and CD84. Grey histograms as indicated in A, and brown histograms represent the expression on MCMVwt and MCMVΔm138 IC-21 infected cells. (C) IC-21 cells were mock-transfected or transfected with the m138-GFP construct or with the control GFP empty vector and stained with the anti-ICOSL mAb or an isotype control (dotted lines). Dark green and red histograms represent cells from transfected cultures expressing or not expressing GFP, respectively, and grey histograms represent surface expression of ICOSL on untransfected cells. In A, B, and C, the isotype for each antibody was used as a negative control (dotted lines). Data are representative of at least two independent experiments.

Figure 3. Localization of m138 in MCMV infected cells. (A) NIH3T3 cells were infected with MCMV-GFP at an moi of 5 for 24 h, fixed with 4% formaldehyde (panels d-f) or fixed and permeabilized with 0.05% Triton (panels a-c and g), and stained with the anti-m138 mAb followed by an anti-mouse IgG-A555. Nuclei were stained with the DAPI reagent. The cells were examined under a fluorescence microscope. Magnification, x20 (a-f); an enlarged individual cell from panel c is shown in panel g. (B) MCMVwt-infected NIH3T3 cells were examined by flow cytometry for surface expression of m138 with the anti-m138 mAb (red histogram). Dotted line represents the

isotype control. (C) 300.19 cells untransfected or stably transfected with the HA-m138 construct were fixed with 4% formaldehyde and stained with the anti-m138 mAb and DAPI and examined under a fluorescence microscope as indicated in A. Magnification, x20. Overlaid images are shown. Transfected cells from the same cultures were analyzed by flow cytometry (right panels) with the anti-m138 mAb (red histogram), an anti-HA mAb (grey histogram) or isotype controls (dotted lines). (D) NIH3T3 cells were infected with MCMV at an moi of 5 for 24 h, treated with LysoTracker DND99, fixed with 4% formaldehyde and permeabilized with 0.02% Saponin, and stained with the anti-m138 mAb followed by an anti-mouse IgG-A488. Nuclei were stained with the DAPI reagent. The cells were examined under a confocal microscope. Representative fields are shown in panels a, b, and c, with an enlargement of an individual and more exposed cell from panel c, in panel d. Magnification, x63.

The online version of this article includes the following figure supplements for figure 3:

Figure supplement 1. **Localization of m138 in MCMV-infected DC2.4 cells.**

Figure 4. m138 leads to a reduction of the expression of ICOSL on the cell surface of infected cells but not of its overall intracellular levels. (A) NIH3T3 cells stably transfected with HA-ICOSL were mock-infected (grey histograms) or infected with MCMVwt or MCMVΔm138 (brown or pink histograms, respectively) and analyzed by flow cytometry for surface expression of ICOSL and MHC I. (B) NIH3T3 HA-ICOSL cells non-transfected (grey histograms) or transfected with the m138-GFP construct (green histograms) were analyzed by flow cytometry for surface expression of ICOSL and CD44. In A and B, the isotype for each antibody was used as a negative control (dotted lines). (C) NIH3T3 HA-ICOSL cells were mock-infected (lane 2), treated with trypsin (lane 3), or infected with MCMVwt (lane 4) or MCMVΔm138 (lane 5).

Untransfected NIH3T3 cells were used as a control (lane 1). Samples were analyzed by western blot using an anti-HA mAb, followed by anti-rabbit IgG-HRP. An anti-IE1 and an anti-actin mAbs followed by anti-mouse IgG-HRP, were used as controls of MCMV infection and loading, respectively. (D) Flow cytometry analysis of NIH3T3 HA-ICOSL treated with trypsin (open histogram) or mock-treated (grey histogram) and stained with an anti-HA mAb or an isotype control (dotted line), followed by anti-mouse IgG PE. (E) NIH3T3 cells (lane 1) or NIH3T3 HA-ICOSL (lane 2) were surface labeled with biotin, immunoprecipitated with an anti-HA mAb, and analyzed by western blot analysis using streptavidin-HRP conjugate. (F) NIH3T3 HA-ICOSL cells were mock-infected (lane 2), or infected with MCMVwt (lane 3) or MCMVwt UV-inactivated (lane 4). Samples were lysed and processed as indicated in C. A lysate of untransfected NIH3T3 cells (lane 1) was also subjected to western blot and employed as a control. All infections were performed at an moi of 5 for 24 h. Data are representative of at least two independent experiments. In C, E, and F, the size of the bands corresponding to ICOSL are indicated on the right margin in kilodaltons (kDa). In E, the sizes of the molecular weight markers are shown on the left side.

Figure 5. m138 impedes ICOSL maturation redirecting it to lysosomal degradation. (A) Western blot analysis of NIH3T3 cells untransfected (lane 1) or transiently co-transfected with either the HA-ICOSL and the control-GFP (CTL-GFP) constructs (lanes 2 and 3), or the HA-ICOSL and the m138-GFP constructs (lanes 4 and 5) and, when indicated, treated with 250 μM of leupeptin and 20 nM of bafilomycin A1 (lanes 3 and 5). The expression of ICOSL and actin was assessed as described in Figure 4C, and for the expression of the m138-GFP and CTL-GFP proteins a polyclonal antibody anti-GFP followed by anti-rabbit IgG-HRP were used. (B) NIH3T3 HA-

ICOSL were infected with MCMVwt at an moi of 5 for 24 h in the absence (-; panels a, b, c and d) or presence of leupeptin and bafilomycin (panels e, f, g and h). Cells were fixed, permeabilized, and stained with anti-m138 and anti-ICOSL mAbs followed by an anti-mouse IgG-A555 and anti-rat IgG-A488, respectively. Nuclei were stained with the DAPI reagent and samples were examined under a confocal fluorescence microscope. Shown are representative cells from cultures stained for m138 (panels a, e), ICOSL (b, f), and overlaid images (c, d, g, and h). Enlarged and more exposed individual cells from panels c and g are presented on panels d and h, respectively. Magnification, x63. (C) NIH3T3 HA-ICOSL infected and treated with the lysosomal inhibitors as in B were fixed, permeabilized with the Foxp3 staining buffer set, and analyzed by flow cytometry with anti-m138 and anti-ICOSL mAbs followed by an anti-mouse IgG-A555 and anti-rat IgG-A488, respectively. Conditions were analyzed in triplicates and median fluorescence intensity (MFI) values +/- SD were extracted from pre-gated m138 positive cells. (D) NIH3T3 cells were co-transfected with the m138-GFP and HA-ICOSL constructs. HA-ICOSL was immunoprecipitated from 0.5% Triton treated lysates using an anti-HA mAb or an anti-hFc as a control. Recovered immunoprecipitates were subjected to SDS-PAGE and western blotting with antibodies against GFP and HA, as described in A and Figure 4C. Data are representative of at least two independent experiments. In A and D, the size of the two bands corresponding to ICOSL, and in D, the band corresponding to m138-GFP, are indicated on the right margin in kilodaltons (kDa). In A and D, the sizes of the molecular weight markers are shown on the left side.

Figure 6. Identification of the m138 domains involved in the downmodulation of ICOSL and CD80. (A) Schematic representation (not drawn to scale) of m138-GFP

protein mutants. NIH3T3 ICOSL-HA cells were untransfected or transfected with m138-GFP, or m138-GFP mutant constructs and analyzed by flow cytometry for ICOSL and CD80 surface levels. Panels on the right represent the MFI of each sample minus the MFI of the control isotypes. Grey histograms represent the expression of untransfected cells and colored histograms represent the expression of cells transfected with m138-GFP (green), m138ΔIg1-GFP (brown), m138ΔIg2-GFP (blue), or m138ΔIg2/3-GFP (red). The isotype for each antibody was used as a negative control (dotted lines). A representative experiment out of two performed is shown.

Figure 7. m138 is capable to restrict $CD8^+$ T-cell activation by downregulating ICOSL on the surface of APCs. (A) C57BL/6 derived BMDCs were mock-infected or infected for 24 hours with MCMVwt or MCMVm138 mutants at an moi of 3 and analyzed by flow cytometry for surface expression of ICOSL and CD80 using specific mAbs against each of these molecules. Grey histograms represent the expression of mock-infected cells and colored histograms represent the expression of cells infected (positive for the MCMV m04 protein) with MCMVwt (yellow), MCMVΔm138 (pink), MCMVm138ΔIg2 (blue), or MCMVm138ΔIg2/3 (red). The isotype for each antibody was used as a negative control (black line histograms). Panels on the right represent the MFI of each sample minus the MFI of the control isotypes. Results are representative of two independent experiments (B) On the left, schematic representation of the *in vitro* antigen-presentation assay. BMDCs infected as indicated in A with MCMVwt (yellow), MCMVΔm138 (pink), MCMVm138ΔIg2 (blue), or MCMVm138ΔIg2/3 (red), or left uninfected (grey) were further co-cultured with naïve $CD8^+$ T cells from Maxi mice. After 6 h, IFN-γ production by $CD8^+$ T cells was determined by flow cytometry. Results

1558 are representative of three independent experiments. Results are expressed as the mean
1559 +/-SEM of the percentage values obtained for samples in each group.
1560
1561 **Figure 8. Via targeting ICOSL, m138 reduces T-cell mediated control of MCMV**
1562 **infection *in vivo*.** (A) BALB/c mice were intraperitoneally (i.p.) inoculated with $2x10^6$
1563 PFU MCMV-GFP. 2 days post infection mice were sacrificed and peritoneal exudate
1564 cells were extracted and analyzed by flow cytometry for surface expression of ICOSL
1565 and MHCI, using specific mAbs against each of these molecules. Blue histograms
1566 represent the expression of uninfected (GFP-) cells and green histograms represent the
1567 expression of MCMV-infected (GFP+) cells from the same mouse. The isotype for each
1568 antibody was used as a negative control (dotted lines). The results obtained from a
1569 representative infected mouse out of two are shown. (B) BALB/c mice (n=4/group)
1570 were mock-infected or i.p. infected with $1x10^6$ PFU of MCMVwt or MCMVΔm138. At
1571 six hpi, peritoneal exudate cells were extracted and surface expression of ICOSL and
1572 CD80 assessed by flow cytometry on the surface of DCs ($CD11^+$ MHC II^+ $CD3^-CD19^-$
1573 $NKp46^-$ cells), gating on m04 positive cells when derived from MCMVwt- or
1574 MCMVΔm138-infected mice. Results are expressed as the mean +/-SD of the MFI
1575 values obtained for samples from two independent experiments. (C) Table displaying
1576 the immunomodulatory effects of the different MCMVs on the cellular targets of m138.
1577 (D) On the top, a schematic representation of the MCMVΔm138 and MCMVm138ΔIg2
1578 *in vivo* infection assay is shown. C57BL/6 mice (n=5-7/group) with or without NK, or
1579 NK, $CD4^+$ and $CD8^+$ T-cell depletion, as indicated, were intravenously (i.v.) inoculated
1580 with $2x10^5$ PFU/mouse of MCMVwt (yellow circles), MCMVΔm138 (pink triangles) or
1581 MCMVm138ΔIg2 (blue triangles). At day 14 post infection mice were sacrificed and
1582 viral titers in salivary glands and lungs of individual mice were determined by standard

plaque assays. Horizontal bars indicate the median values. The Kruskal-Wallis test was used to assess statistical differences between experimental groups. *p<0.05, **p<0.01. A representative experiment out of two performed is shown.

The online version of this article includes the following figure supplements for figure 8:

Figure supplement 1. **m138 contributes to immune evasion of $D4^+$ T cells in spleens and lungs of MCMV infected mice.**

Figure 9. Blockade of ICOSL reduces the frequency of particular lymphocyte subsets in the spleen and lymph nodes of MCMV infected mice. (A) BALB/c mice (n=11-12/group) were i.p. inoculated with $2x10^6$ PFU of MCMVΔm138 and treated with (α-ICOSL) or without (CTL) 100 mg of anti-ICOSL mAb. At day 14 post infection mice were sacrificed, and spleens and lymph nodes were isolated and disaggregated. Cell suspensions were analyzed by flow cytometry using anti-mouse CD3, CD4, CD8, CD44, CD62L, CXCR5 and PD1 for T-cell phenotype. For B cell phenotype B220, CD21, CD23, CD95 and GL7 mAbs were used. Percentages of Tfh cells ($CD3^+CD4^+CXCR5^{hi}PD1^{hi}$), germinal center (GC) B cells ($CD95^{hi}GL7^{hi}B220^+$), follicular (FO) B cells ($CD21^+CD23^+B220^+$), and $CD3^+CD4^+$ or $CD3^+CD8^+$ naïve ($CD44^{low}CD62L^{hi}$) and memory ($CD44^{hi}CD62L^{low}$) T cells from these two organs are shown. (B) Representative immunofluorescence of spleens from mice infected and treated with (panels b and d) or without (panels a and c) the anti-ICOSL mAb, as indicated in A. Two color colocalization with B220 in green and peanut agglutinin (PNA) in red are shown at x4 and x10 magnifications. Panels on the right show a graphic representation of follicle and germinal center relative areas from tissue sections of a representative mouse of each experimental group. In graphs shown in A and B, results are expressed as mean +/- SD. Mice treated with anti-ICOSL mAb are

represented as red squares and mice not receiving the mAb are represented as open circles. Two-tailed unpaired *t*-tests were used to assess statistical differences between experimental groups. *p<0.05, **p<0.01, ***p<0.001, ****p<0.0001. Data are pooled from two independent experiments.

The online version of this article includes the following figure supplements for figure 9:

Figure supplement 1. **Effect of ICOSL blockade on the frequency of several lymphocyte subsets in the spleen and lymph nodes of MCMV infected mice.**

Figure 10. ICOSL blockade limits the generation of MCMV specific antibodies. (A) Total levels of IgG, IgG1, IgG2a, IgG2b, IgG3 (at dilutions 1:200 and 1:400), and IgM (at dilutions 1:25 and 1:50) were determined by ELISA from sera collected at day 14 of the same infected BALB/c mice indicated in Figure 8A. (B) Sera (at dilutions 1:10 and 1:100) as in A were tested in a viral neutralization assay. Results are presented as the percentage of plaque reduction determined by the ratio of the number of plaques counted in the sample wells relative to the ratio of plaques in wells containing the serum of an uninfected mouse used as a negative control. In A and B, results are expressed as mean +/- SD. Mice treated with anti-ICOSL mAb are represented as red squares and mice that did not receive the mAb are represented as open circles. Two-tailed unpaired *t*-tests were used to assess statistical differences between experimental groups. *p<0.05, **p<0.01, ***p<0.001. Data are pooled from two independent experiments.

The online version of this article includes the following figure supplements for figure 10:

Figure supplement 1. **Effect of ICOSL blockade on MCMV neutralization in the presence of complement.**

Figure 11. HCMV, HSV-1, and HSV-2 also limit cell surface expression of ICOSL on APCs. (A) Primary monocyte-derived macrophages (upper panels) and PMA-treated THP-1 cells (bottom panels) were mock-infected or infected for 72 hours with HCMV-GFP at an moi of 10 and analyzed by flow cytometry for cell-surface expression of human ICOSL or CD70 using specific mAbs against each of these receptors. Gray histograms represent the expression of mock-infected cells, green histograms represent the expression on HCMV-infected (GFP+) cells, and blue histograms represent the expression on uninfected (GFP-) cells from the same culture. (B) PMA-treated THP-1 cells were mock-infected (time 0) or infected with HCMV-GFP as in A and analyzed by flow cytometry for surface expression of ICOSL at the different time points after infection indicated. (C) Same as in A, except that an moi of 20 was used, and THP-1 cells were also exposed for 72 h to the same amount of HCMV-GFP UV-inactivated (red histogram). (D) Equal amounts of lysates from PMA-treated THP-1 cells mock-infected (lane 1) or infected for 72 h at an moi of 20 with HCMV-GFP (lanes 2 and 3), and when indicated, treated with 250 μM leupeptin and 20 nM of bafilomycin A1 (lane 3), were lysed and analyzed by western blot with antibodies against ICOSL and actin, followed by anti-rabbit IgG-HRP (ICOSL) or anti-mouse IgG-HRP (actin). (E) PMA-treated THP-1 cells were mock-infected or infected with HSV-1-GFP, HSV-1-GFP UV-inactivated, HSV-2-GFP or HSV-2-GFP UV-inactivated at an moi of 100 (HSV-1) or 200 (HSV-2). 24 h later the expression of human ICOSL and CD70 were analyzed as in A. Green histograms represent the expression of ICOSL on infected cells, red histograms represent the expression on UV-inactivated HSV infected cells, and grey histograms represent the expression on mock-infected cells. The isotype for the ICOSL antibody was used as a negative control (dotted lines). A representative experiment out of three performed is shown. (F) PMA-treated THP-1 cells were mock-infected (lane 1)

or infected with HSV-1-GFP (lane 2) and HSV-2-GFP (lane 3) as indicated in E. Cell lysates were prepared, and subjected to western blot analysis using an anti-human ICOSL or anti-actin mAbs as in D. The molecular weight of the band corresponding to ICOSL is indicated in D and E in kilodaltons on the right margin.

Figure 3-figure supplement 1. Localization of m138 in MCMV-infected DC2.4 cells. D2.4 cells were infected with MCMV-GFP at an moi of 5 for 24 h, fixed with 4% formaldehyde, permeabilized with 0.05% Triton, and stained with the anti-m138 mAb followed by an anti-mouse IgG-A555. Nuclei were stained with the DAPI reagent. The cells were examined under a fluorescence microscope. Magnification, x20 (a-c); an enlarged individual cell from panel c is shown in panel d.

Figure 8-figure supplement 1. m138 contributes to immune evasion of $D4^+$ T cells in spleens and lungs of MCMV infected mice. On the top, a schematic representation of the adoptive transfer *in vivo* assay is shown. $1x10^5$ M25-specific transgenic $CD4^+$ T cells were transferred (i.v.) into C57BL/6 SCID mice (n=4-5/group), which were depleted of NK cells as indicated, and either mock-infected or i.p. infected with $2x10^5$ PFU/mouse of MCMVwt or MCMVΔm138. Seven dpi, spleens, lungs and salivary glands were harvested, and analyzed by flow cytometry using anti-CD45.1 and anti-CD4 specific mAbs. The frequency of $CD45.1^+$ $CD4^+$ cells for each organ is indicated. Results are expressed as the mean +/-SEM of the percentage values obtained for samples in each group.

Figure 9-figure supplement 1. Effect of ICOSL blockade on the frequency of several lymphocyte subsets in the spleen and lymph nodes of MCMV infected mice.

Cell suspensions obtained from spleens and lymph nodes of BALB/c mice infected and treated as indicated in Figure 8A were analyzed by flow cytometry using anti-mouse CD3, CD4, CD8, CD5, B220, CD23, CD21, CD138, and CD19 mAbs, and anti-mouse IgM polyclonal Ab. Percentages of total B cells ($B220^{+}$), marginal zone (MZ) B cells ($CD21^{+}CD23^{-}B220^{+}$), B1 B cells ($CD19^{hi}B220^{int}$), B1a ($CD19^{hi}B220^{int}CD5^{+}$) and B1b ($CD19^{hi}B220^{int}CD5^{-}$) subsets, $CD3^{+}CD4^{+}$ or $CD3^{+}CD8^{+}$ T cells, and plasma cells ($CD138^{hi}B220^{low}CD19^{-}IgM^{-}$) are shown. Results are expressed as mean +/- SD. Mice treated with anti-ICOSL mAb are represented as red squares and mice untreated are represented as open circles. Two-tailed unpaired *t*-test was used to assess statistical differences between experimental groups.

Figure 10-figure supplement 1. Effect of ICOSL blockade on MCMV neutralization in the presence of complement. Same as in Figure 9B, except that the MCMV neutralization assay was performed in the presence of rabbit complement. Results are presented as the percentage of plaque reduction determined by the ratio of the number of plaques counted in the sample wells relative to the ratio of plaques in wells containing the serum of an uninfected mouse used as a negative control. Results are expressed as mean +/- SD. Mice treated with anti-ICOSL mAb are represented as red squares and mice untreated are represented as empty circles. Two-tailed unpaired *t*-test was used to assess statistical differences between experimental groups. *$p<0.05$, **$p<0.01$.

Supplementary File 1. Key Resources Table.

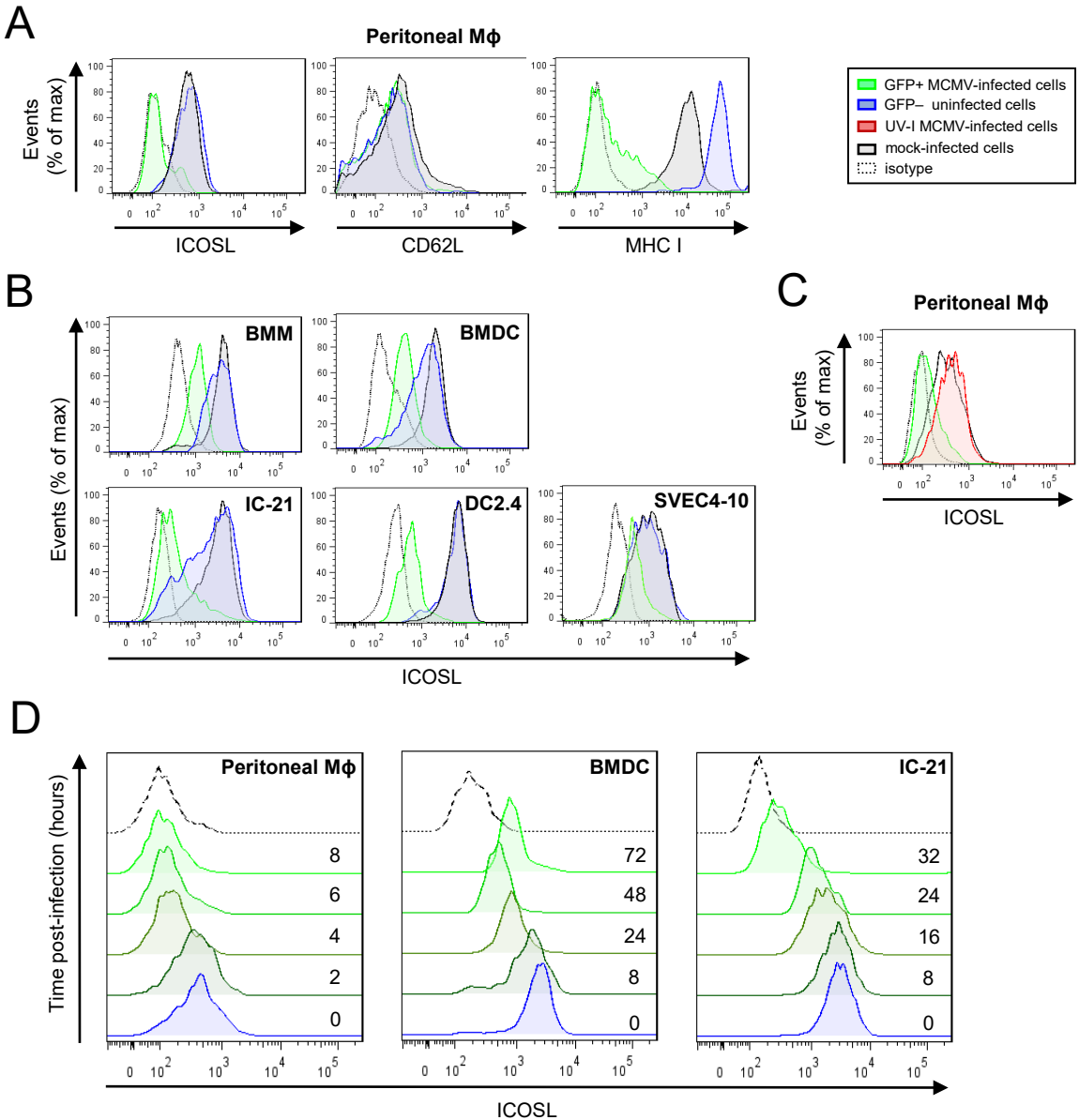
A
Peritoneal Mϕ
Events (% of max)
ICOSL
CD62L
MHC I
GFP+ MCMV-infected cells
GFP– uninfected cells
UV-I MCMV-infected cells
mock-infected cells
isotype
B
BMM
BMDC
IC-21
DC2.4
SVEC4-10
Events (% of max)
ICOSL
C
Peritoneal Mϕ
Events (% of max)
ICOSL
D
Peritoneal Mϕ
BMDC
IC-21
Time post-infection (hours)
8
6
4
2
0
72
48
24
8
0
32
24
16
8
0
ICOSL

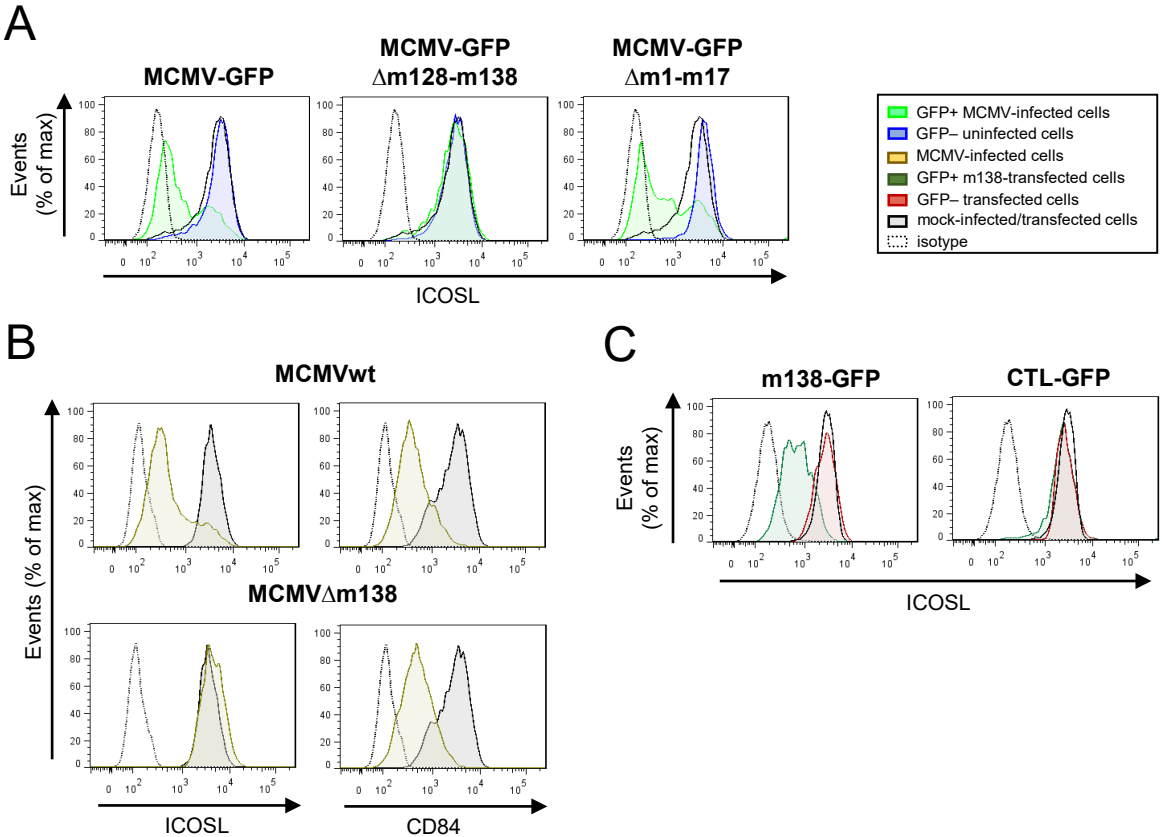
A
MCMV-GFP
MCMV-GFP Δm128-m138
MCMV-GFP Δm1-m17
Events (% of max)
ICOSL
GFP+ MCMV-infected cells
GFP– uninfected cells
MCMV-infected cells
GFP+ m138-transfected cells
GFP– transfected cells
mock-infected/transfected cells
isotype
B
MCMVwt
MCMVΔm138
Events (% of max)
ICOSL
CD84
C
m138-GFP
CTL-GFP
Events (% of max)
ICOSL

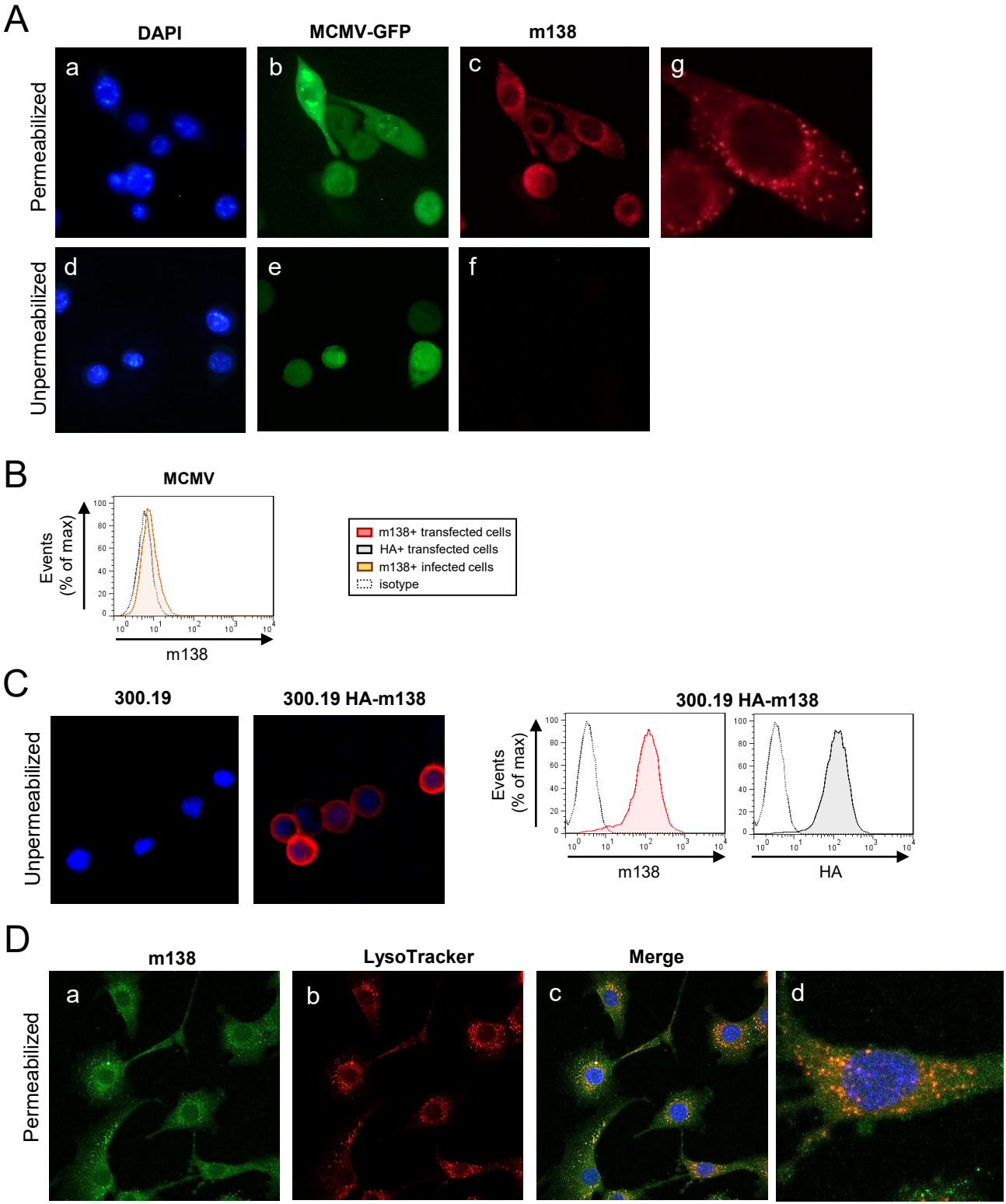
A
DAPI
MCMV-GFP
m138
Permeabilized
Unpermeabilized
a
b
c
g
d
e
f
B
MCMV
Events (% of max)
m138
m138+ transfected cells
HA+ transfected cells
m138+ infected cells
isotype
C
300.19
300.19 HA-m138
Unpermeabilized
300.19 HA-m138
Events (% of max)
m138
HA
D
m138
LysoTracker
Merge
Permeabilized
a
b
c
d

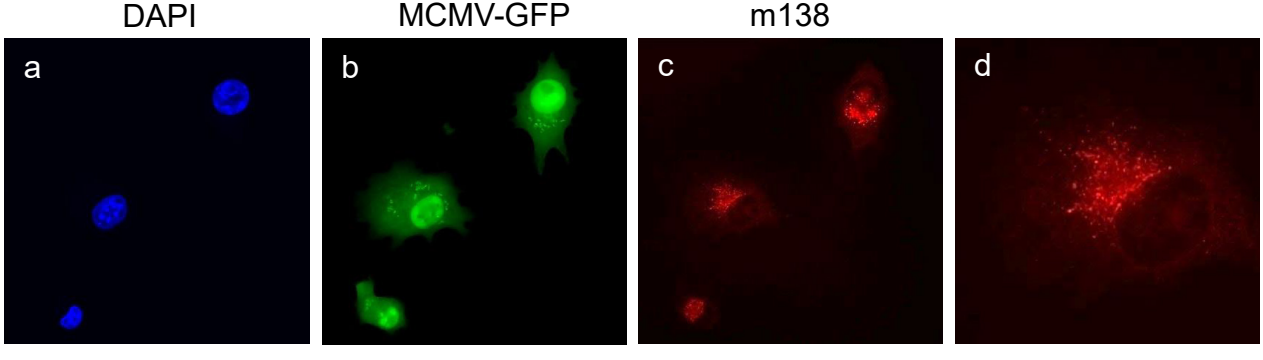
DAPI
MCMV-GFP
m138
a
b
c
d

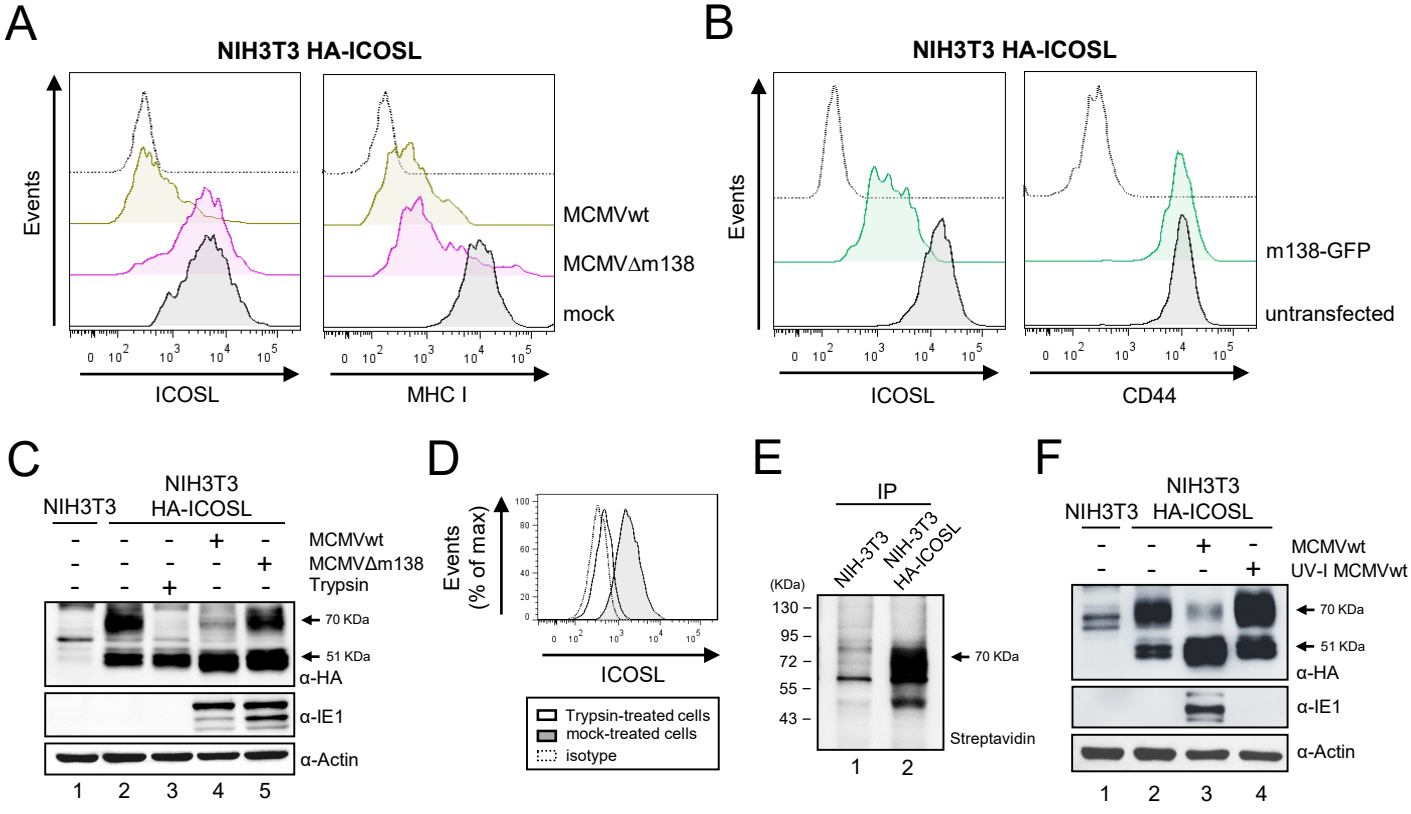
A
NIH3T3 HA-ICOSL
Events
MCMVwt
MCMVΔm138
mock
ICOSL
MHC I
B
NIH3T3 HA-ICOSL
Events
m138-GFP
untransfected
ICOSL
CD44
C
NIH3T3
NIH3T3 HA-ICOSL
MCMVwt
MCMVΔm138
Trypsin
70 KDa
51 KDa
α-HA
α-IE1
α-Actin
1 2 3 4 5
D
Events (% of max)
ICOSL
Trypsin-treated cells
mock-treated cells
isotype
E
IP
NIH-3T3
NIH-3T3 HA-ICOSL
(KDa)
130
95
72
55
43
70 KDa
Streptavidin
1 2
F
NIH3T3
NIH3T3 HA-ICOSL
MCMVwt
UV-I MCMVwt
70 KDa
51 KDa
α-HA
α-IE1
α-Actin
1 2 3 4

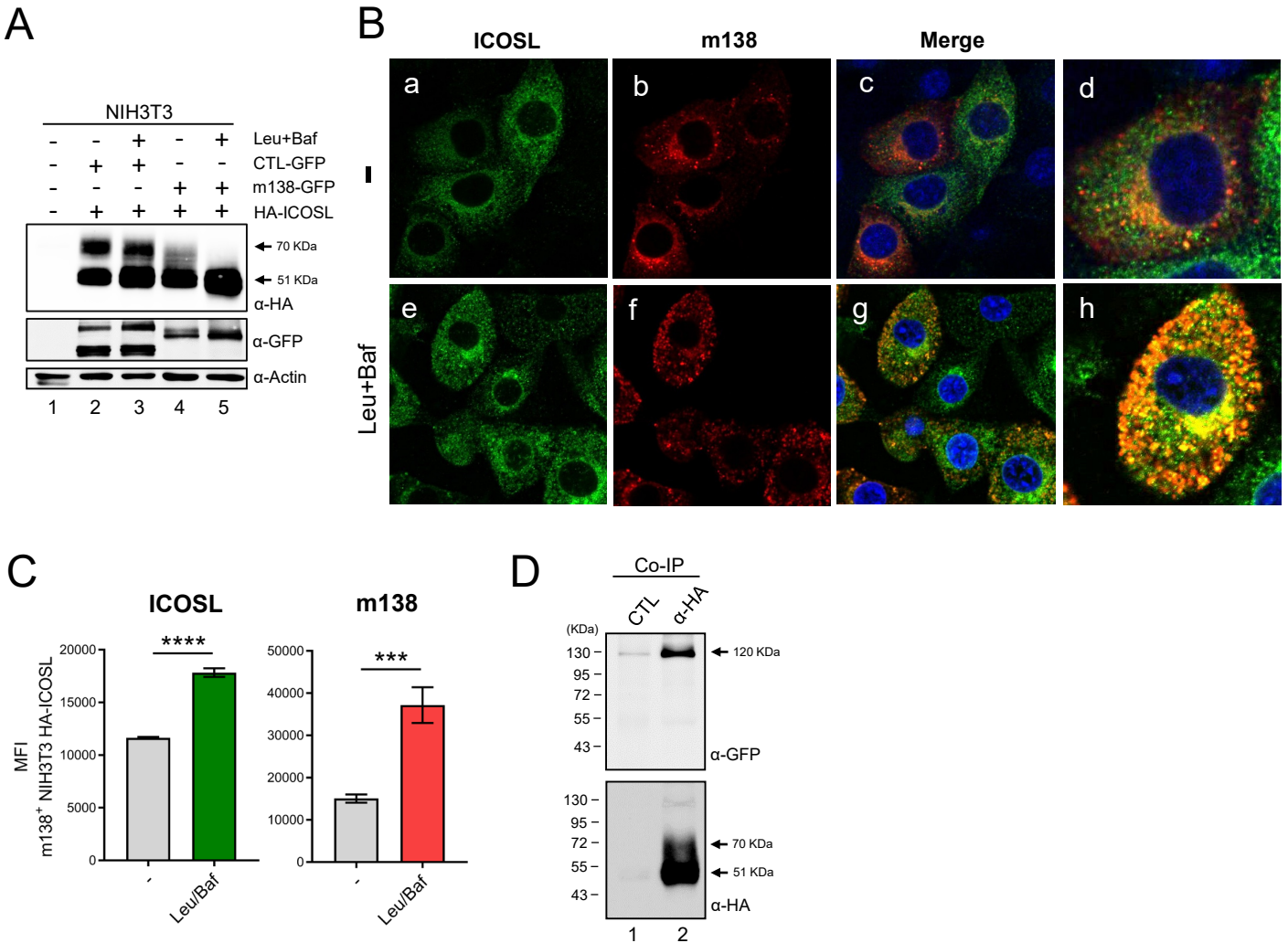
A
NIH3T3
- - + - + Leu+Baf
- + + - - CTL-GFP
- - - + + m138-GFP
- + + + + HA-ICOSL
70 KDa
51 KDa
α-HA
α-GFP
α-Actin
1 2 3 4 5
B
ICOSL
m138
Merge
a
b
c
d
e
f
g
h
-
Leu+Baf
C
ICOSL
m138
****
***
MFI
m138+ NIH3T3 HA-ICOSL
20000
15000
10000
5000
0
50000
40000
30000
20000
10000
0
-
Leu/Baf
D
Co-IP
CTL
α-HA
(KDa)
130
95
72
55
43
120 KDa
α-GFP
70 KDa
51 KDa
α-HA
1 2

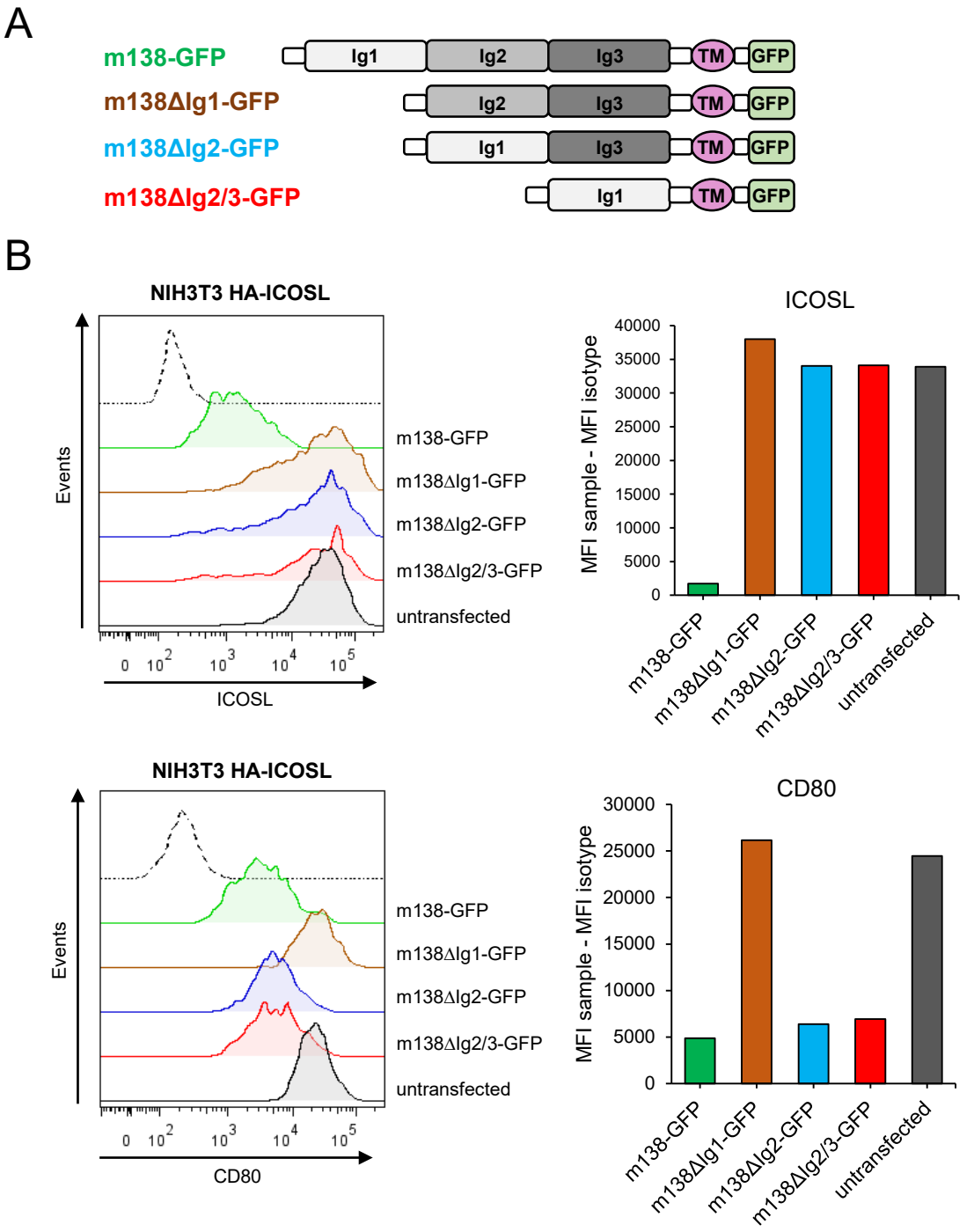
A
m138-GFP
Ig1
Ig2
Ig3
TM
GFP
m138ΔIg1-GFP
m138ΔIg2-GFP
m138ΔIg2/3-GFP
B
NIH3T3 HA-ICOSL
Events
m138-GFP
m138ΔIg1-GFP
m138ΔIg2-GFP
m138ΔIg2/3-GFP
untransfected
0 10^2 10^3 10^4 10^5
ICOSL
ICOSL
MFI sample - MFI isotype
40000
35000
30000
25000
20000
15000
10000
5000
0
m138-GFP
m138ΔIg1-GFP
m138ΔIg2-GFP
m138ΔIg2/3-GFP
untransfected
NIH3T3 HA-ICOSL
Events
m138-GFP
m138ΔIg1-GFP
m138ΔIg2-GFP
m138ΔIg2/3-GFP
untransfected
0 10^2 10^3 10^4 10^5
CD80
CD80
MFI sample - MFI isotype
30000
25000
20000
15000
10000
5000
0
m138-GFP
m138ΔIg1-GFP
m138ΔIg2-GFP
m138ΔIg2/3-GFP
untransfected

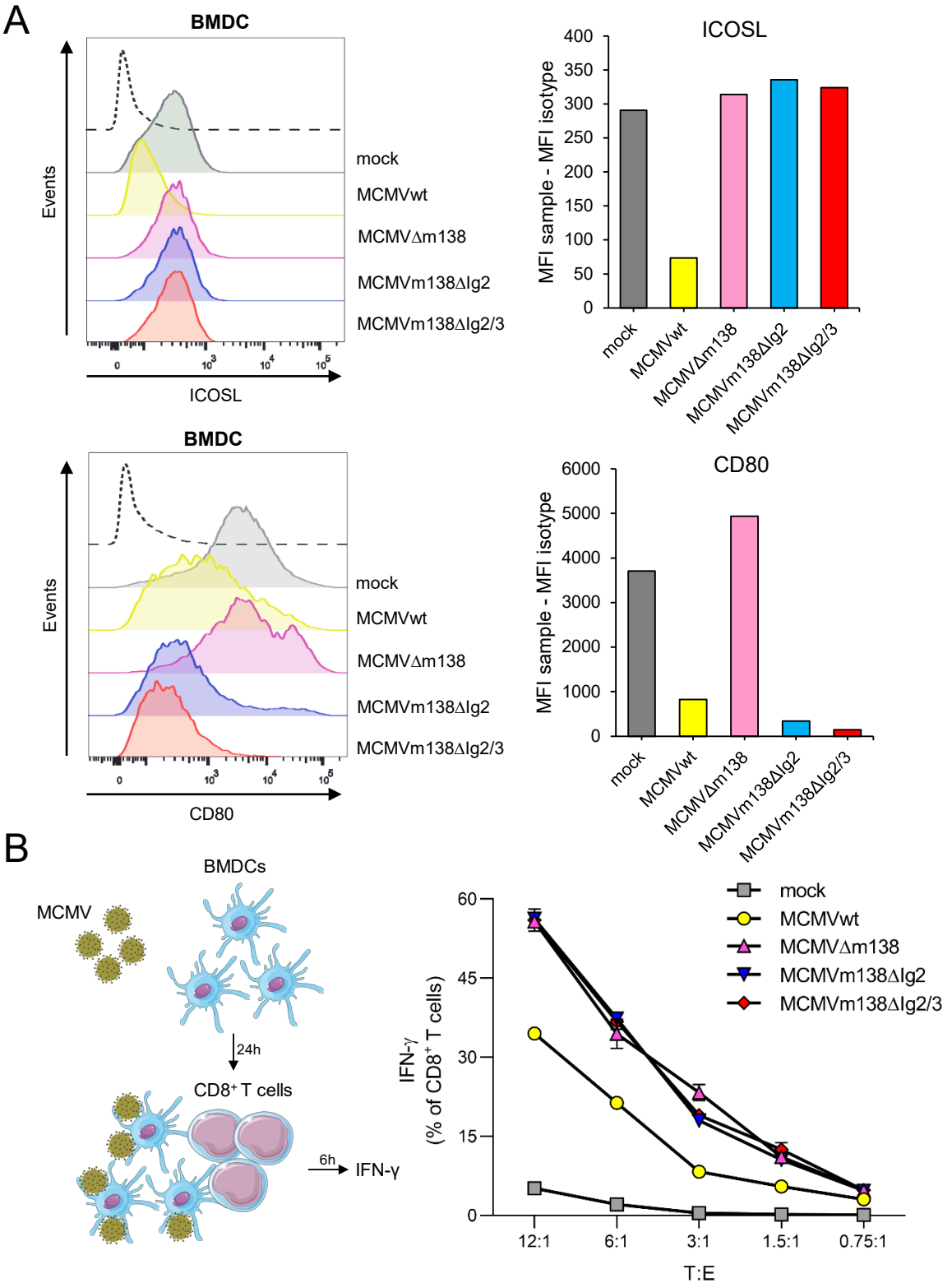
A
BMDC
Events
mock
MCMVwt
MCMVΔm138
MCMVm138Δlg2
MCMVm138Δlg2/3
ICOSL
ICOSL
MFI sample - MFI isotype
mock
MCMVwt
MCMVΔm138
MCMVm138Δlg2
MCMVm138Δlg2/3
BMDC
Events
CD80
CD80
MFI sample - MFI isotype
B
BMDCs
MCMV
24h
CD8+ T cells
6h
IFN-γ
IFN-γ
(% of CD8+ T cells)
T:E
12:1
6:1
3:1
1.5:1
0.75:1

A

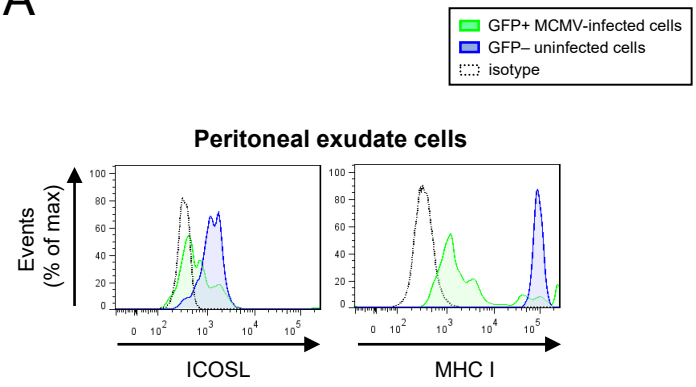

B

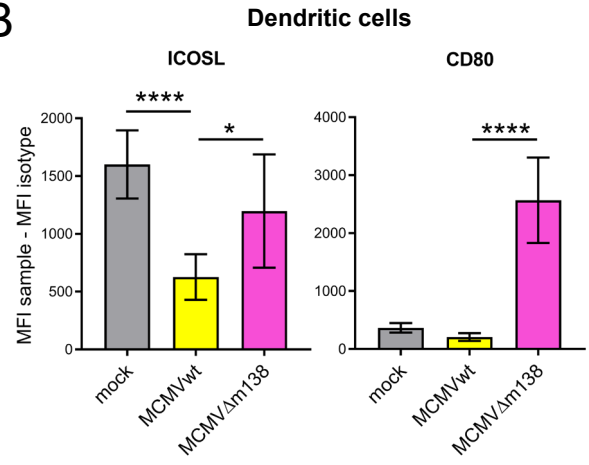

C

	NKG2D ligands			co-stimulatory molecules	
Viruses	MULT-1	RAE-Iε	H60	ICOSL	CD80
MCMVwt (full lenght m138)	downregulated	downregulated	downregulated	downregulated	downregulated
MCMVΔm138 (m138 deleted)	not altered	not altered	not altered	not altered	not altered
MCMVm138ΔIg2 (m138 Ig2 domain deleted)	downregulated	downregulated	not altered	not altered	downregulated

Effects of MCMVwt and mutants on m138 targets at the surface of infected cells

D

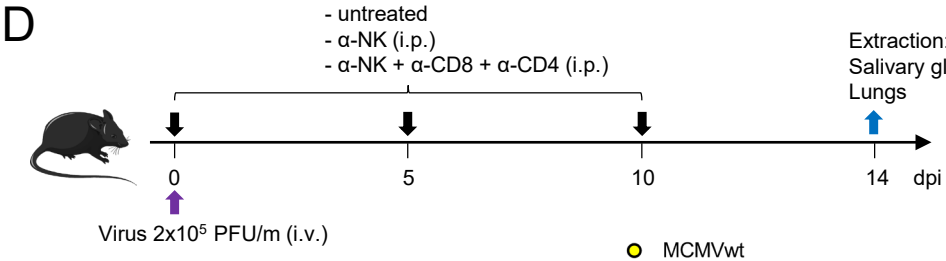

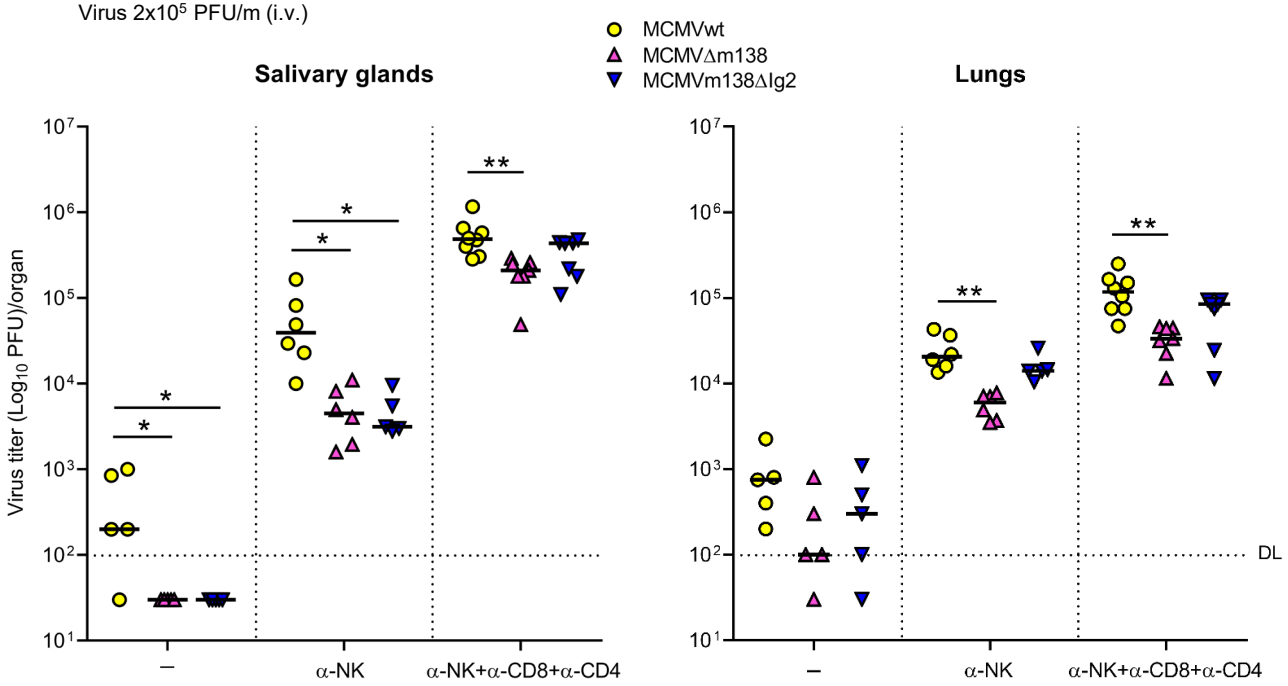

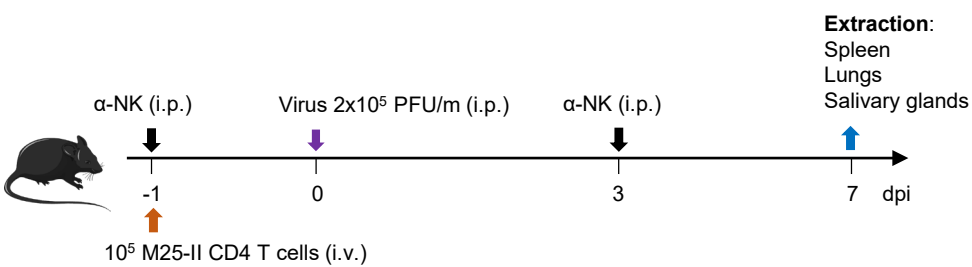
Extraction:
Spleen
Lungs
Salivary glands
α-NK (i.p.)
Virus 2x10⁵ PFU/m (i.p.)
α-NK (i.p.)
-1
0
3
7
dpi
10⁵ M25-II CD4 T cells (i.v.)

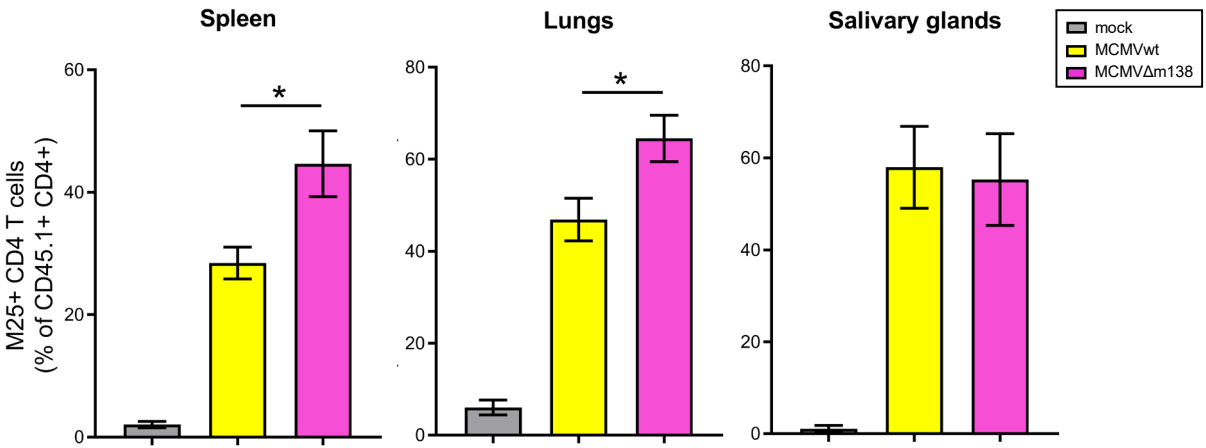
Spleen
Lungs
Salivary glands
mock
MCMVwt
MCMVΔm138
M25+ CD4 T cells
(% of CD45.1+ CD4+)
0
20
40
60
80
*
*

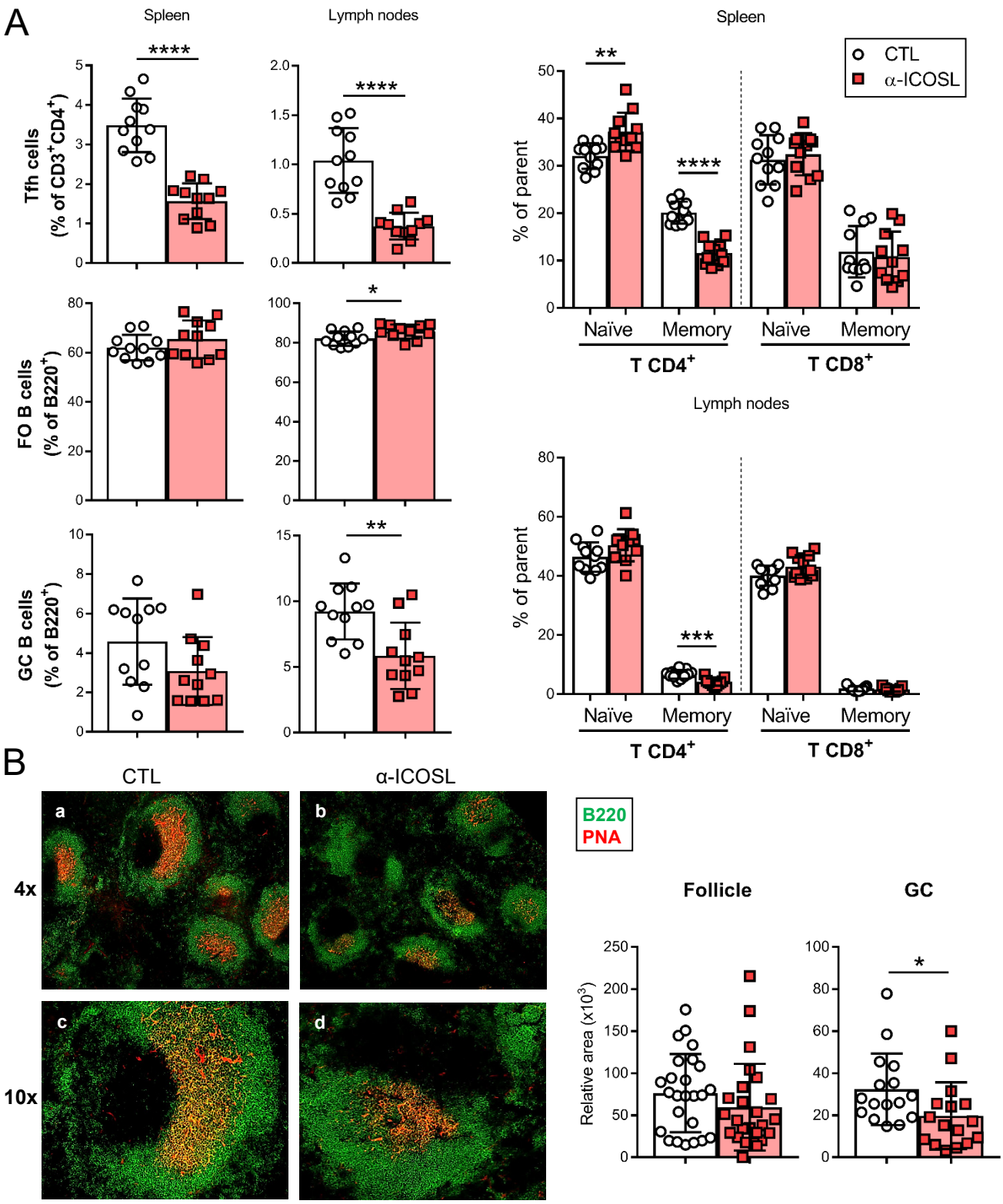
A
Spleen
Lymph nodes
Tfh cells
(% of CD3+CD4+)
FO B cells
(% of B220+)
GC B cells
(% of B220+)
****
****
*
**
Spleen
CTL
α-ICOSL
% of parent
**
****
Naïve
Memory
Naïve
Memory
T CD4+
T CD8+
Lymph nodes
% of parent
***
Naïve
Memory
Naïve
Memory
T CD4+
T CD8+
B
CTL
α-ICOSL
a
b
c
d
4x
10x
B220
PNA
Follicle
GC
Relative area (x10³)
*

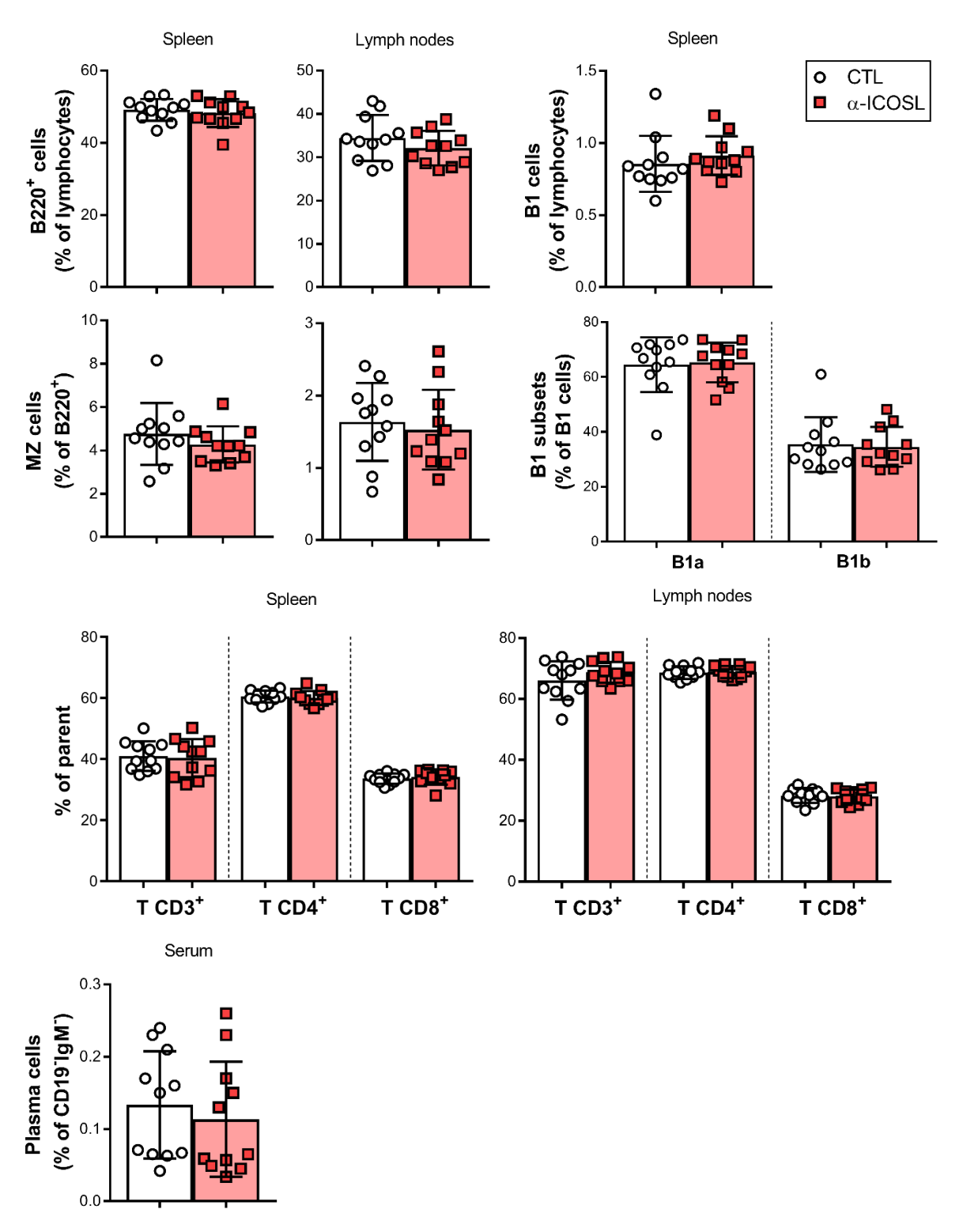
Spleen
Lymph nodes
Spleen
CTL
α-ICOSL
B220+ cells (% of lymphocytes)
B1 cells (% of lymphocytes)
MZ cells (% of B220+)
B1 subsets (% of B1 cells)
B1a
B1b
Spleen
Lymph nodes
% of parent
T CD3+
T CD4+
T CD8+
Serum
Plasma cells (% of CD19+IgM-)

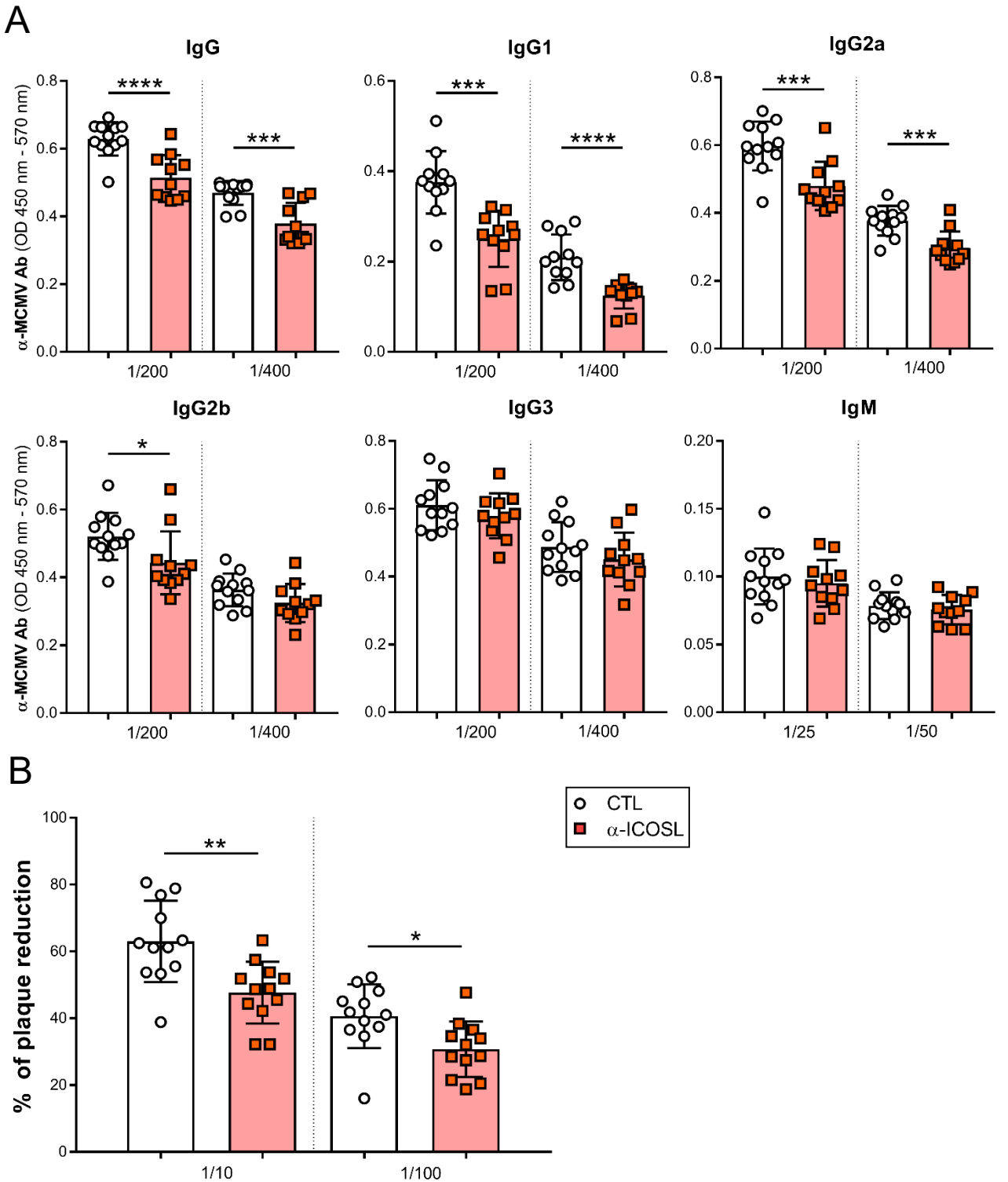
A
IgG
IgG1
IgG2a
IgG2b
IgG3
IgM
α-MCMV Ab (OD 450 nm - 570 nm)
****
***
*
1/200
1/400
1/25
1/50
B
% of plaque reduction
**
1/10
1/100
CTL
α-ICOSL

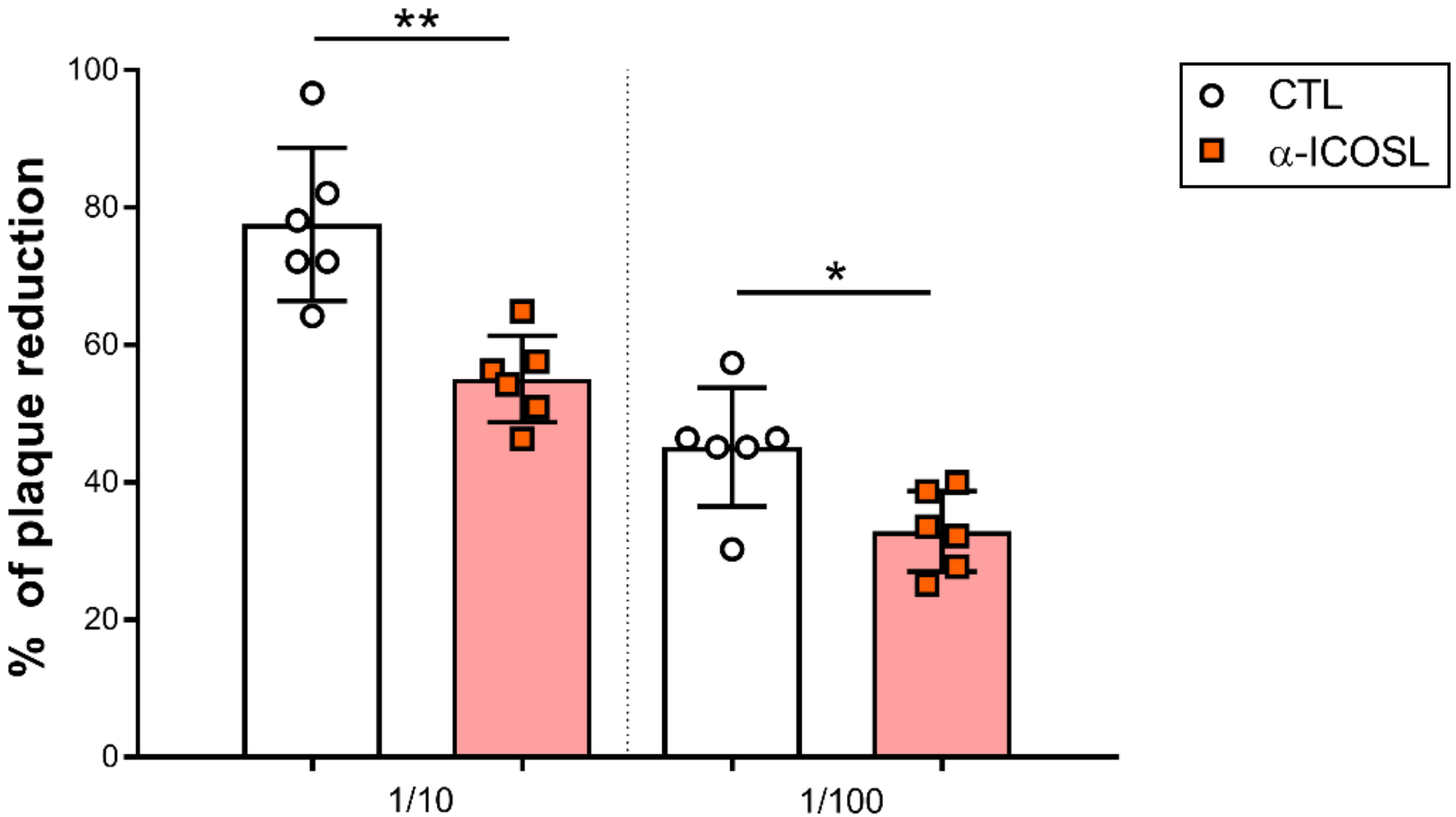
**
*
100
80
60
40
20
0
% of plaque reduction
1/10
1/100
CTL
α-ICOSL

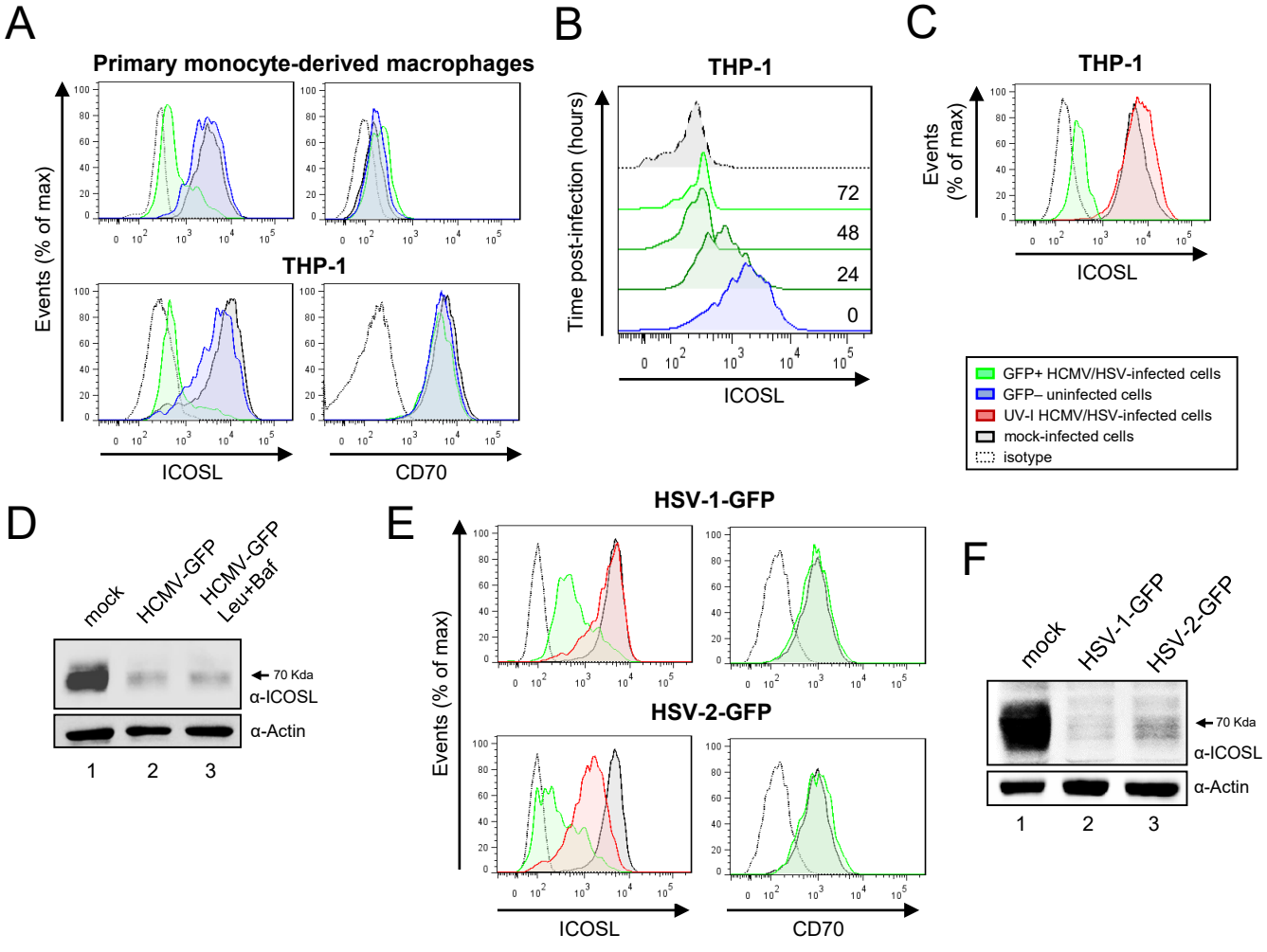
A
Primary monocyte-derived macrophages
THP-1
Events (% of max)
ICOSL
CD70
B
THP-1
Time post-infection (hours)
72
48
24
0
ICOSL
C
THP-1
Events (% of max)
ICOSL
GFP+ HCMV/HSV-infected cells
GFP– uninfected cells
UV-I HCMV/HSV-infected cells
mock-infected cells
isotype
D
mock
HCMV-GFP
HCMV-GFP Leu+Baf
70 Kda
α-ICOSL
α-Actin
1
2
3
E
HSV-1-GFP
HSV-2-GFP
Events (% of max)
ICOSL
CD70
F
mock
HSV-1-GFP
HSV-2-GFP
70 Kda
α-ICOSL
α-Actin
1
2
3